UCL Université catholique de Louvain

École polytechnique de Louvain (EPL)

# Adaptive control during reaching movements in humans

Dissertation presented by
**Marie BASTIN**

for obtaining the Master's degree in
**Biomedical Engineering**

Supervisor(s)
**Frédéric CREVECOEUR, Philippe LEFÈVRE**

Reader(s)
**Frédéric CREVECOEUR, Philippe LEFÈVRE , André MOURAUX**

Academic year 2017-2018

# Acknowledgments

I would like to thank my thesis advisors professor Philippe Lefèvre and professor Frédéric Crevecoeur for their time and their precious advice through the process of researching and writing this thesis.

I would also like to thank professor Jean-Louis Thonnard for its guidance regarding the anatomical aspect of this thesis.

I would also like to acknowledge professor André Mouraux as the third reader of this thesis.

I would like to thank my friends and family who gave their time and took part to the experiment, without whom this thesis would not have been possible.

I would finally like to thank my parents and my sister for their unconditional support throughout my years of study.

# Contents

# Introduction

Living our everyday lives requires to constantly interact with our environment. For example, reaching for objects with our upper limbs is a very common thing to do and seems to be a quite simple task since everyone manages to successfully perform it. Indeed, children start to reach for objects that interest them at about the age of 3 months [1]. However, even if reaching for an object feels very natural and easy, the completion of such a task actually requires that our CNS (Central Nervous System) computes correctly and rapidly enough the motor commands that will produce the desired arm motion. In other words, the motor controller of the CNS must be able to somehow invert the relationship between the force generated by the muscles and the resulting produced movement of the limb. This is far from easy. To do so, it is necessary to build up an internal model of the dynamics of the environment we are evolving in. For example, we know that it is harder to lift a bucket full of water than an empty bucket, and therefore we produce a higher effort to lift the full bucket. If our CNS was not able to estimate the difference of weight between an empty and a full bucket, we would produce the same effort in both cases and the effort produced to lift the full bucket would not be sufficient.

We constantly interact with different environment dynamics and the environment dynamics can also change very quickly. Some changes can be anticipated. For example, the dynamics of our upper limb changes when we grasp an object and displace it to another location. Some changes are on the contrary totally unexpected. Indeed, our movements can be disturbed through shocks, for example when we rush into someone, when we sit in an unstable train, etc... Those changes in our environment dynamics could represent a big issue for our motor controller but humans are actually known to excel in the ability to adapt rapidly to the variable dynamics of their arm as the hand interacts with the environment [1]. For example, if we are holding a drink in a crowd, we will not necessarily spill it if someone pushes our arm: we will instead stabilize our arm and restore our balance.

Discovering how the CNS builds up internal models of our environment and updates it according to the dynamical changes of the environment represents an outstanding challenge in the understanding of motor control and motor adaptation. Expanding our knowledge about human motor control could have important impacts on other scientific fields, for example in robotics where the development of humanoid robots and their accurate motor control represent a tremendous challenge. We also hope for clinical application in a nearby future.

The present work is a contribution to the understanding of the strategies established by the CNS to correct for disturbances during reaching movements in humans. The current study was motivated by the results and the conclusions of a previous one, namely: *A sub-movement time scale of human motor adaptation*[2]. The main contribution of this work is to reproduce the behavioural results and analyze muscle activity to gain better insight into the timescale of the underlying process.

This dissertation is organized as follows: we first go through some concepts and the review of the literature in the contextual setting; the materials and methods are then described; we then

present all the results before discussing them and we finally reach the conclusion.

# Chapter 1

# Contextual setting

## 1.1 Useful concepts

I will first of all go over some concepts that are important for the understanding of the study.

### 1.1.1 Motor adaptation

From our birth and during our whole lifetime, we are confronted to novel environments and it is necessary to learn how to interact with it. This learning process is called motor adaptation and is a form of motor learning, described as a process of acquiring motor skills through adaptive representations.[3] When we are confronted to a new environment, it is very likely that the motor commands computed by the CNS will not be adapted to the dynamics conditions of that environment, leading to errors in the kinematics of our movements. For example, moving into water is different from moving through air. If we tried to perform accurate movements the first time we were immersed into water, we would experience difficulties and find ourselves incapable of doing it. However, if we spend enough time practicing into water, we will eventually recover our motor skills. In other words, our CNS is able to learn the dynamics of a new environment in order to integrate internal models of that environment so that we are able to compute a motor command to perform a desired motion. Another example of adaptation is how we learn to control a body that changes over time: aging over long time scales and fatigue over short time scales require adaptation to changes in dynamics.

There are currently two different explanations to the phenomenon of motor adaptation. The first one stipulates that our CNS adapts to the environment so that it eliminates the kinematic errors, in comparison to the baseline kinematic performed in the normal environment. This however implies a strong hypothesis that each task has one corresponding optimal kinematics, no matter the environment dynamics [4],[5]. Another point of view is to think the motor adaptation as a process of re-optimization. Through reward-based optimization, we use the internal model to search for a better movement plan to minimize implicit motor costs and maximize rewards. [6] This second approach allows the possibility that a new environment might induce a different optimal kinematics.

There are currently two main techniques to study motor adaptation during reaching movements. The first one is to perturb the visual consequence of a motor command while keeping the proprioceptive consequences untouched. This technique is called the visuomotor adaptation.[7] In this work, we used the second paradigm, which consists in physically perturbing the participant, which influences the proprioceptive and the visual consequences of a motor command. This second paradigm is called force-field adaptation. [7]

### 1.1.2 Adaptive control

An adaptive controller is a type of controller that allows to deal with uncertainties. These uncertainties take two forms: the parameters of the controller are variable, or the initial parameters of the controller are unknown. For example, a mass of a flying plane is a variable parameter, since it will decrease as the plane's motors consume fuel. An adaptive controller should be able to automatically adjust itself in real time in order to achieve or to maintain a desired level of control system performance. [8]

An adaptive system must be capable of performing the following functions: providing continuous information about the present state of the system or identifying the process; comparing present system performance to the desired or optimum performance and making a decision to change the system to achieve the defined optimum performance; and initiating a proper modification to drive the control system to the optimum. [9]

An adaptive controller can either be direct or indirect. Indirect methods estimate the parameters in the plant and further use the estimated model information to adjust the controller while direct methods are ones wherein the estimated parameters are those directly used in the adaptive controller. [10]

To this day, the vast majority of studies in the field of motor adaptation or skill learning have focused on trial-by-trial acquisition of motor skills through learning curves. The main motivation for studying adaptive control is that this framework considers real-time adjustments of motor commands to unexpected changes in dynamics.

### 1.1.3 Internal model

Figure 1.1 shows the typical structure of a feedback controller in motor control. The feedback controller relies on the computation of an error to compute the motor command. The error is defined as the difference between the desired trajectory and the realized trajectory. The motor command can then be computed through a proportional, an integral or a derivative feedback controller. The computation of the error comes with a delay.

In human motor control, the delay to compute the error between the desired and the realized trajectories is very large in comparison to the movement duration. Indeed, the delay of visual feedback on arm movements ranges from 150-250 ms while spinal feedback loops require 30-50 ms time delay.[11] Knowing that very fast movements last about 150 ms, these can not be properly executed relying solely on feedback control, even if the mechanical properties of muscles produce proportional (stiffness) and derivative (viscosity) gains without delay.[11]

This leads to the following explanation: the internal model hypothesis depicted in Figure 1.2 proposes that the brain needs to acquire an inverse dynamics model of the object to be controlled through motor learning, after which motor control can be executed in a pure feedforward manner.[11]

Forward internal models can predict sensory consequences from efference copies of motor commands whereas inverse internal models, on the other hand, can calculate necessary feedforward motor commands from desired trajectory information.[11]

Interacting with our environment is based on predictions (feedforward) and perceptions (feedback). Another advantage of feedforward models is that if our predictions are unbiased, then

what we perceive will be more accurate if we integrate our predictions with the measurements of our sensory system.[7] In other words, our ability to interact with our environment is based on the combination of feedforward and feedback controllers which improve each others performances.

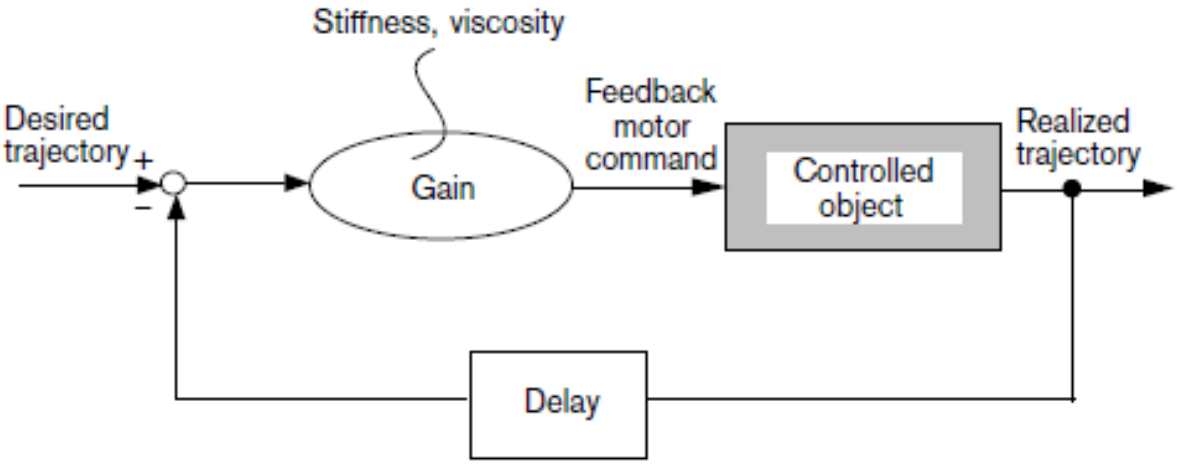


Figure 1.1: Feedback control. Image taken from: [11]

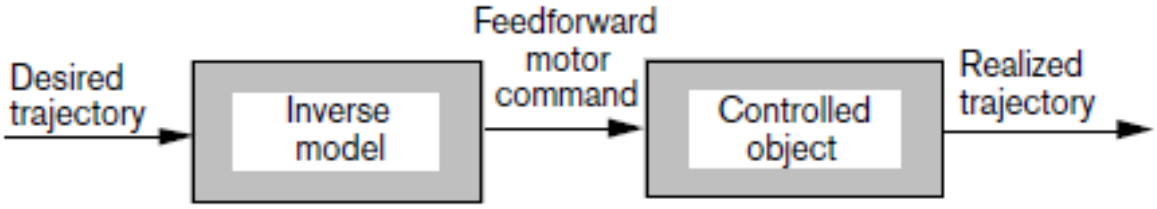


Figure 1.2: Internal model. Image taken from: [11]

## 1.2 Overview of the literature

### 1.2.1 Reza Shadmehr and Ferdinando A. Mussa-lvaldi, 1994: a pioneer study

I describe here the article of Reza Shadmehr and Ferdinando A. Mussa-lvaldi, 1994, namely: *Adaptive Representation of Dynamics during Learning of a Motor Task.*[1] Their goal was to understand how the motor control deals with new dynamics of the arm. The participants performed reaching movements while holding the end-effector of a manipulandum. This manipulandum could apply forces proportional to the hand velocity and therefore disturb the movement of the participants. The workspace of the reaching movements was divided into two parts: the left workspace and the right workspace.

They first studied the trajectories performed by the participants with no perturbation and with perturbation. Figure 1.3 shows the results that they obtained. In the baseline condition, participants approximately followed a straight line from the starting point to the target. Under the force field, the trajectories of the participants had the typical form of a "hook".

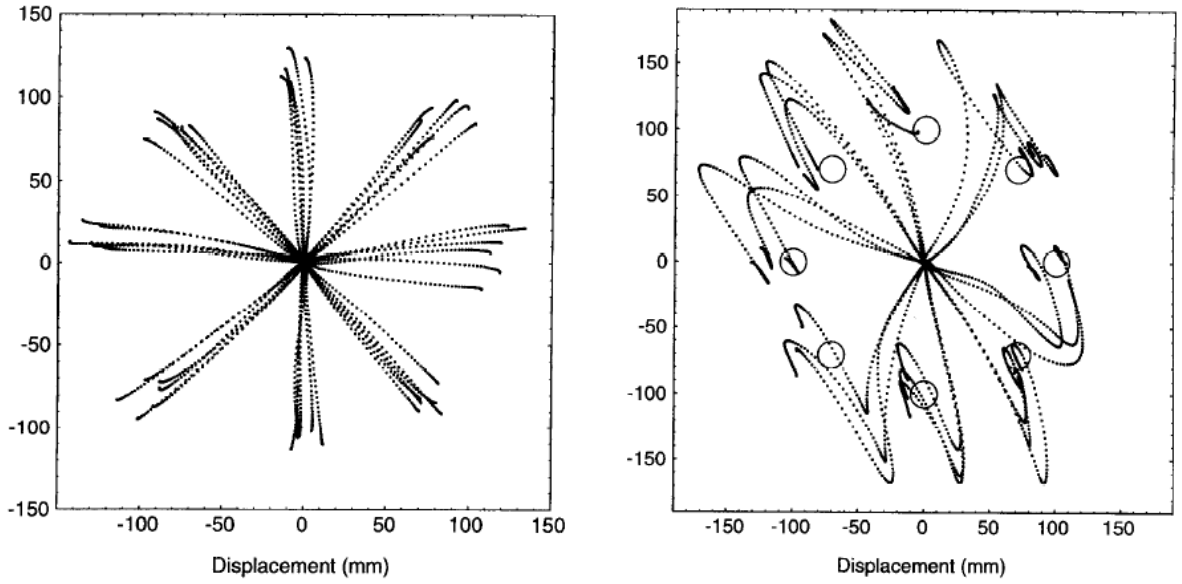


Figure 1.3: Left: hand trajectories at the right workspace in a null force field. Right: Trajectories at the right workspace during first perturbation. Image taken from: [1]

Afterwards, they made the participants train in the force field condition and they observed that they progressively recovered the trajectories obtained when no perturbation was applied. This result is a clear example of motor adaptation.

The authors then explored the possibility that this motor adaptation was explained by the development of an internal model of the force field. This suggestion is an alternative to another explanation: co-activation of the muscles would make the movements insensitive to external forces.

They made the participants perform reaching movements under the force field (training period) and randomly made them perform reaching movements in the null field. They observed trajectories, name *aftereffects*, which were qualitatively "opposite" to the ones obtained during the first exposure to the perturbation. The "magnitude" of those aftereffects also increased with the training period. This result supports the idea that the CNS built an internal model of the force field. Indeed, the hypothesis that the co-activation of the muscles corrected the trajectory can not explain the presence of the aftereffects once the force field was removed.

Next, the authors tried to understand the structure of the internal model. They tested the hypothesis that the internal model was based on a local association between states and forces. To do so, they asked the participants to perform null field reaching movements in the left workspace, before and after a training period in the right workspace. They found out that there were aftereffects in the left workspace following the training period in the right workspace. This result indicates that the hypothesis that the internal model was based on a local association between states and forces is wrong.

Finally, the authors concluded from their study that during adaptation to a force field that significantly changes the dynamics of a reaching movement, the CNS forms an internal model of the added dynamics. This internal model has the power to generalize well beyond the training region.[1]

### 1.2.2 From then to now

In 2001, Etienne Burdet, Rieko Osu, David W. Franklin, Theodore E. Milner and Mitsuo Kawato explored the possibility that stability during reaching movements was ensured by the control of mechanical impedance, specifically the spring-like property of muscles.[12] To do so, they made participants perform reaching movements under an unstable dynamics environment. They concluded from their results that stability was achieved by optimizing the magnitude, the shape and the orientation of impedance. They confirmed their results in a following paper in 2007.[13]

In 2003, Kan Singh and Stephen H. Scott explored how the brain maps limb motion and requisite muscular forces during motor skill acquisition.[14] They made participants perform reaching movements under disturbing force fields either proportional to elbow or shoulder velocity. Their results indicate that when facing uncertainties, the chosen strategy is to associate motor actions at a joint with sensory feedback from that joint.

In their paper *Shared Internal Models for Feedforward and Feedback Control* (2009) [15], Mark J. Wagner and Maurice A. Smith investigated how motor adaptation affects online responses to untrained and unanticipated perturbations in humans. They investigated how newly learned changes in the motor system's internal models for feedforward control of novel dynamics affected feedback control responses. To do so, they made participants learn novel velocity-dependent dynamics and after adaptation, participants undergone occasional force-pulse perturbations which produced unanticipated changes in velocity. They found that as they expected, task-appropriate responses to the perturbations compensated corresponding changes in velocity-dependent dynamics. To accomplish this, the neural processes underlying feedback control must be capable of accurate real-time state prediction for velocity via a forward model and have access to recently learned changes in internal models of limb dynamics.[15]

In 2009, Isaac Kurtzer, J. Andrew Pruszynski and Stephen H. Scott investigated on-line corrections to perturbations during reaching movements in their paper *Long-Latency Responses During Reaching Account for the Mechanical Interaction Between the Shoulder and Elbow Joints.*[16] The participants performed reaching movements and torque perturbations were randomly applied to the shoulder and/or the elbow. The authors studied the response of the long-latency reflex (45-100 ms) of the shoulder to those perturbations. The long-latency reflex is highly flexible and includes the fastest possible contribution from primary motor cortex, a key neural substrate for self-initiated action.[16] Their results showed that the long-latency reflex integrated multi-joints dynamics, i.e. it integrated information from both the shoulder and the elbow. These results support the hypothesis that highly sophisticated feedback control underlies motor behavior and are consistent with a shared neural substrate, such as primary motor cortex, for feedforward and feedback control.[16]

In 2013, Tyler Cluff and Stephen H. Scott explored the hypothesis that feedback responses changed during motor learning in their paper *Rapid Feedback Responses Correlate with Reach Adaptation and Properties of Novel Upper Limb Loads.*[17] Studying how feedback responses adapt to motor adaptation required to find a paradigm where the motor adaptation process did not influence the muscle activity. By maintaining constant elbow muscle activity during reaching movements to a target that only required shoulder motion and by applying novel elbow loads, the authors dissociated adapted feedback responses from altered muscle stiffness or co-activation.[17] They found that participants that adapted more to the load showed greater modulation of their stretch responses, highlighting an important relationship between feedback responses and performance in the adapted motor skill and excluding the possibility that external loads produced nonspecific increases in feedback responses.[17]

In 2014, Joseph Y. Nashed, Frédéric Crevecoeur and Stephen H. Scott investigated how sensory feedback for online movement control influences decision-making between competing movements or goals.[18] To do so, they made participants perform reaching movements with obstacles located on both sides of the straight path connecting the starting and ending points of the task. They then randomly perturbed the limb of the participants with mechanical loads that varied with amplitude and direction. In the first experiment, participants had to reach one single target while in the second experiment they could choose between three targets. The authors found out that the timing of the corrective responses was different between the two experiments. This difference in the timing of the corrective responses suggests that the brain has a hierarchical structure for processing different aspects of motor corrections.

In 2018, Frédéric Crevecoeur, Jean-Louis Thonnard and Philippe Lefèvre investigated the possibility that the nervous system updates its internal representations in real-time following the principles of adaptive control.[2] They made participants perform reaching movements and on random trials, a velocity-dependent force-field was applied to disturb the movement. The participants could not anticipate the perturbation and yet the authors found out that the participants progressively improved the online corrections for the perturbation. This result supports the idea of an online adaptation during reaching movements.

# Chapter 2

# Materials and Methods

## 2.1 Participants

18 participantss, aged from 22 to 59 (11 women and 7 man, 4 left-handed and 14 right-handed) took part to the experiment. All participants were healthy and did not present any history of neuronal illness or neuronal incident. The experiment lasted approximately an hour and a half; the participants were not compensated for their time. The experimental procedures were approved by the ethics committee at the host institution (UCLouvain).

## 2.2 Task

Participants were instructed to sit in front of a robotic device (KINARM, BKIN Technologies, Kingston, Canada: see paragraph **KINARM**) and to grab the right handle of the device with their right hand. They were asked to perform reaching movements towards a visual target. Three types of trials were performed by the participants: the baseline ones where no perturbation was applied and the perturbed trials where an orthogonal force field was applied by the device, either clockwise or counter-clockwise. The force is designed so that it maps the forward hand velocity and is defined as follows:

- Clockwise trials: $F_x = L\dot{y}$ [N]
- Counter-clockwise trials: $F_x = -L\dot{y}$ [N]

  with $L = 13$ [Ns/m].

Each participant performed six blocks of 60 trials, composed of 50 baseline trials randomly interleaved with five clockwise and five counter-clockwise trials.

### 2.2.1 Visual display

The visual display of the experiment is depicted in Figure 2.1.

The starting point is represented by a circle of 6 mm of radius. Its center is located at coordinates (5,10) cm. The target is depicted by a bigger circle of 1.2 cm of radius. It is located at coordinates (5,25) cm. Therefore, 15 cm separate the two circles. When the participant is performing the experiment, he can see the position of its right hand (holding the right handle of the KINARM) in real time. This position is depicted by a small cursor on the screen. The participant is asked to place the cursor inside the starting point and to remain in that position while waiting for the beginning of the trial. This waiting time can vary from 2 to 4 seconds. When the cursor is correctly placed inside the starting point, the latter becomes green, validating

the position (Figure 2.1a).

The target was initially depicted by an empty red circle. When the cursor was correctly placed inside the starting point, the beginning of the trial was visually indicated once the target filled up with red (Figure 2.1b). From that moment, the participant must move its cursor to reach the target within a time interval of 600 ms to 800 ms. If the participant reached the target within that interval, the target turned green, indicating that the trial was a success (Figure 2.1c). If the participant had moved too fast, the target returned to its initial appearance (Figure 2.1a). If the participant had moved too slow, the target remained fully red (Figure 2.1b). Whatever the outcome of the trial, the participant was asked to maintain the position of its cursor inside the target until the end of the trial, which finally happened when both the starting point and the target vanished from the screen.

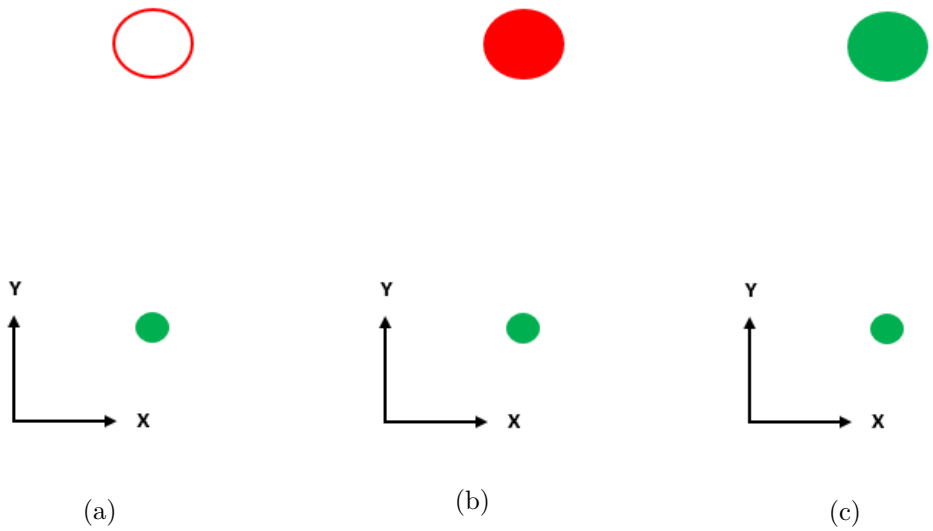


(a) (b) (c)

Figure 2.1: Visual display of the experiment. (a) Visual display when the cursor of the hand is located inside the starting point, waiting for the go signal. (b) The target fills up with red: it is the go signal. (c) The target turns green; indicating that the trial is a success.

## 2.3 Data collection and analysis

### 2.3.1 KINARM

The robotic device (KINARM, BKIN Technologies, Kingston, Canada; see Figure 2.2) allowed the participant to move its arm (shoulder and elbow) in the horizontal plane. It could also apply forces at the handles (see Figure 2.3) in order to displace the participant's arm and to perturb its movement.

Figure 2.2: Representation of the KINARM device. Image taken from: [19]

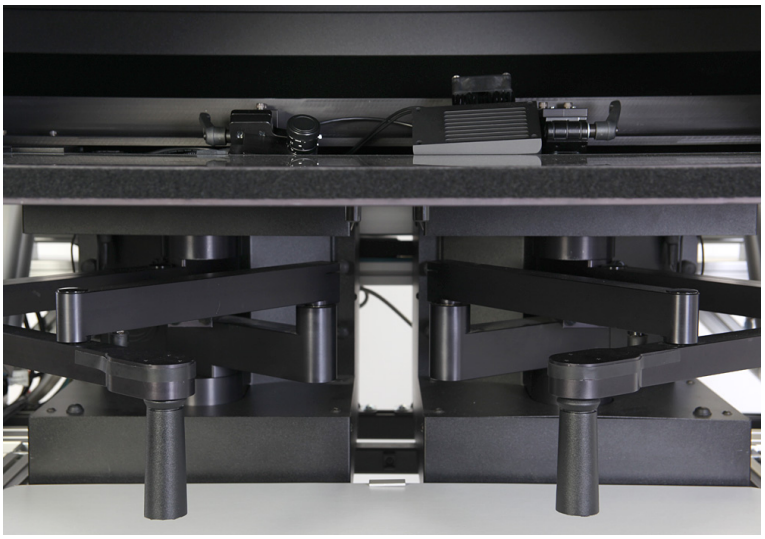

Figure 2.3: Handles of the robotic device. Image taken from: [19]

### 2.3.2 Measured variables

The position (x and y-coordinates) and the force (x and y-coordinates) were measured at the handle of the robotic device. Those signals were sampled at 1 kHz and low-pass filtered (second order Butterworth filter, cut-off frequency of 50 Hz). The velocity (x and y-coordinates) was numerically obtained through finite differences of order two. All signals were aligned on the so-called reference time which corresponds to the 1/3 of the baseline trajectory, as shown on Figure 2.4. All signals were truncated from 1000 ms before the reference time to 1700 ms after the reference time, giving data that expand over 2700 ms.

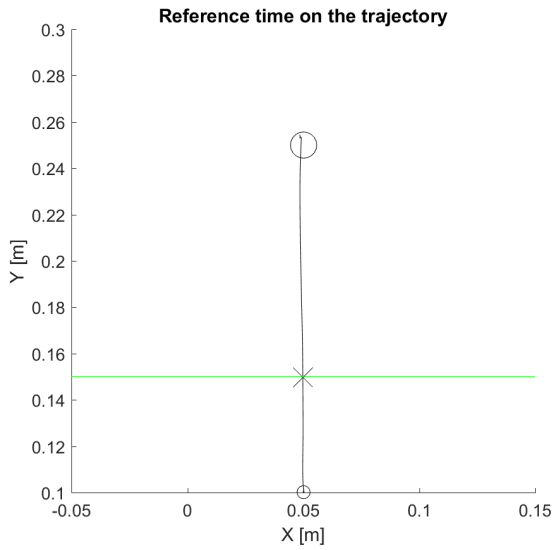


Figure 2.4: Visualization of the reference time on which all signals are aligned. Black line: trajectory; black cross: reference time; Green line: 1/3 of the trajectory.

We analyzed the evolution of the trajectory (x-position in function of y-position) between the first perturbed trial and the last one, for both the clockwise and the counter-clockwise trials. We retrieved two parameters from those trajectories: the overshoot and the maximum deviation. For the clockwise perturbation, the maximum deviation along the x-axis was obtained by taking the maximum component of the x-position vector, while the overshoot was obtained by taking the minimum component of the x-position vector. On the contrary, for the counter-clockwise perturbation, we took the maximum deviation along the x-axis as the minimum component of the x-position vector, and we took the overshoot as the maximum component of the x-position vector.

We analyzed the evolution of the force (x and y-coordinates) between the first perturbed trial and the last one, for both the clockwise and the counter-clockwise trials.

We retrieved the critical times, defined as the moment at which the EMG curves significantly start to differ between the first and the last perturbed trials. We also retrieved the starting times (i.e. the beginning of the movement), defined as the moment at which the participant leaves the starting point.

### 2.3.3 Muscle activity

Muscle activity was recorded from six muscles of the upper-limb by a commercially available system (Bagnoli, Delsys). The signal was also amplified with a gain equal to $10^4$ and digitally sampled at 1000 Hz. For all analysis, the muscle activity was filtered with a band-pass Butterworth filter ([10 400] Hz, 2nd order and dual pass) then normalized to the average activity obtained during calibration trials. All signals were aligned on the reference time and were truncated from 1000 ms before the reference time to 1700 ms after the reference time, giving data that expand over 2700 ms.

#### Calibration

Participants performed two calibration blocks, one at the beginning and the other at the end of the experiment in order to obtain a baseline activity of each recorded muscle. During the

calibration trials, the participants were told to stabilize the position of their hand in the starting point of the visual display (see the green circle in Figure 2.1a) while the robotic device applied a force oriented in one of the four following directions: ± y and ± x. A calibration block was composed of three trials in each direction.

### Choice of the muscles

The task of the experiment was a reaching task in which the participant moved its right arm with two degrees of freedom in an horizontal plane. The participant also experienced force field perturbations oriented either clockwise or counter-clockwise. The goal was to study the muscles which will most likely be recruited during the task. Six muscles were picked: the biceps, the triceps, the infraspinatus, the pectoralis major, the anterior deltoid and the posterior deltoid.

Figure 2.5 shows the biceps brachialis. The principal actions of this muscle are the flexion of the elbow and the supination of the forearm. We expect that this muscle will be recruited during the baseline task and maybe more during the trials where a clockwise perturbation is applied.

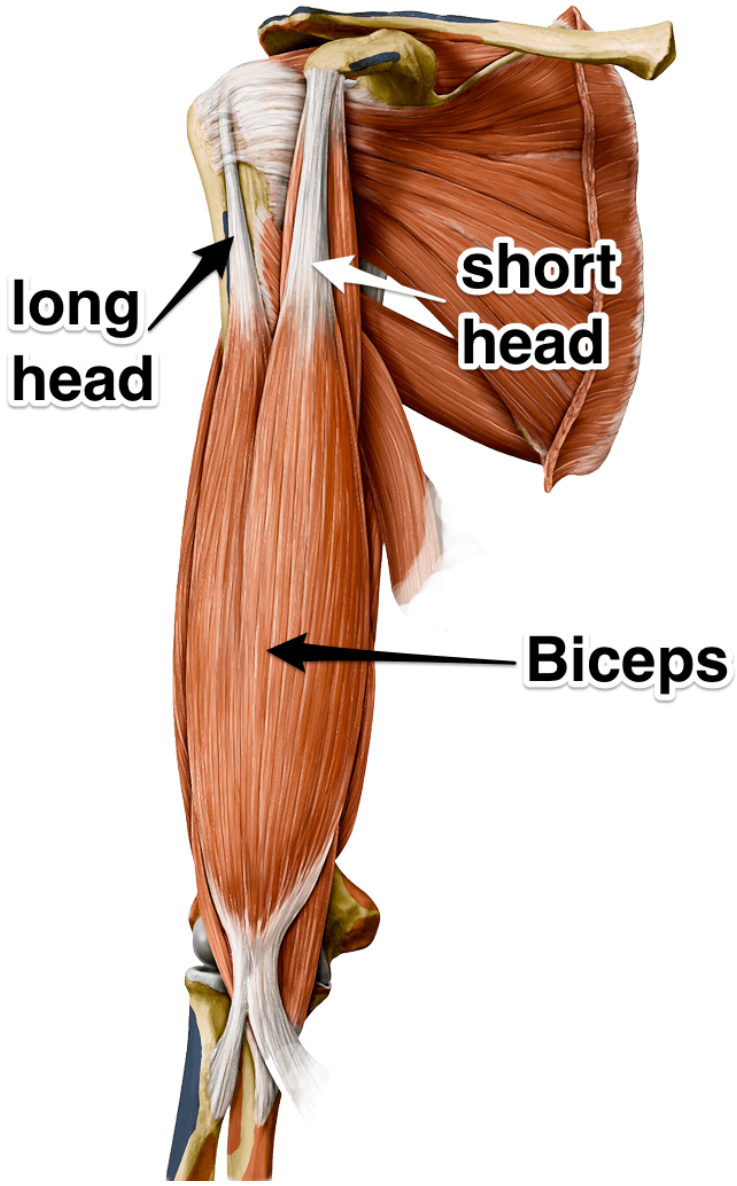


Figure 2.5: Frontal view of the biceps brachialis of the right arm. Image taken from: [20]

The antagonist muscle of the biceps is shown on Figure 2.6: the triceps. Its main action is the extension of the elbow. It should be recruited during the task even if there is no perturbation applied and possibly more when a counter-clockwise force field is applied.

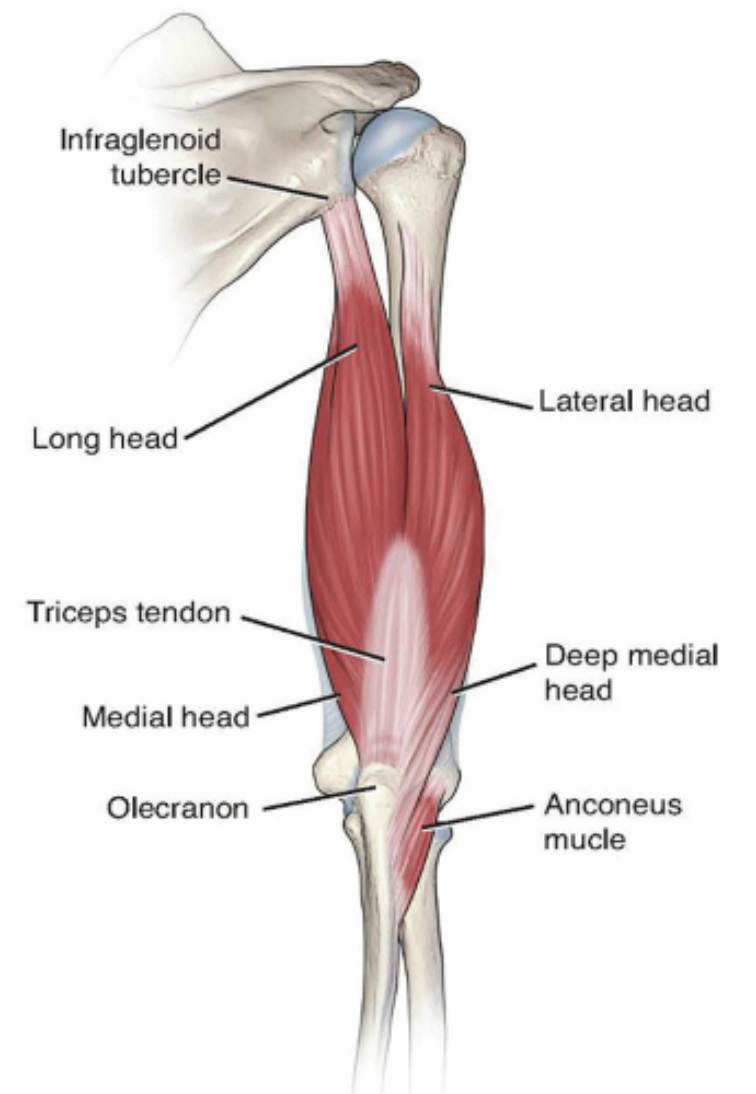


Figure 2.6: Posterior view of the triceps of the right arm. Image taken from: [21]

Figure 2.7 shows the three components of the deltoid muscle. We decided to investigate the anterior and the posterior deltoids. The anterior deltoid is responsible for the flexion and the medial rotation of the arm. It should be particularly recruited when a clockwise perturbation is applied. The posterior deltoid is the antagonist muscle of the anterior deltoid. It is therefore recruited for the extension and the lateral rotation of the arm. In this case we expect to observe a higher activity during the trials where a counter-clockwise force field occurs.

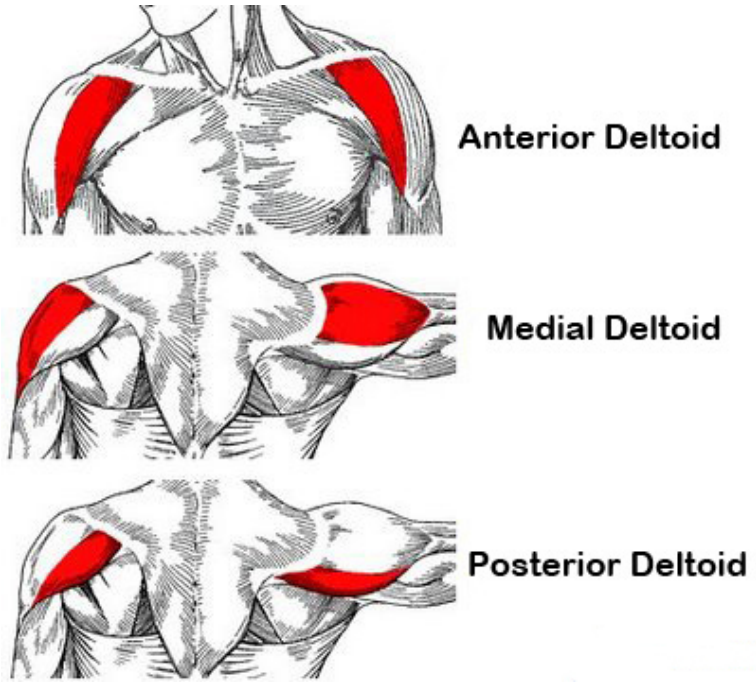


Figure 2.7: Anterior, medial and posterior deltoids. Image taken from: [22]

The pectoralis major muscle is depicted in Figure 2.8. We decided to study the activity of this quite large muscle right under the collarbone. This muscle mainly takes action during the adduction of the arm and the medial rotation of the humerus. Its clavicular part also helps during the flexion of the arm. Its activity should increase when a clockwise perturbation is applied.

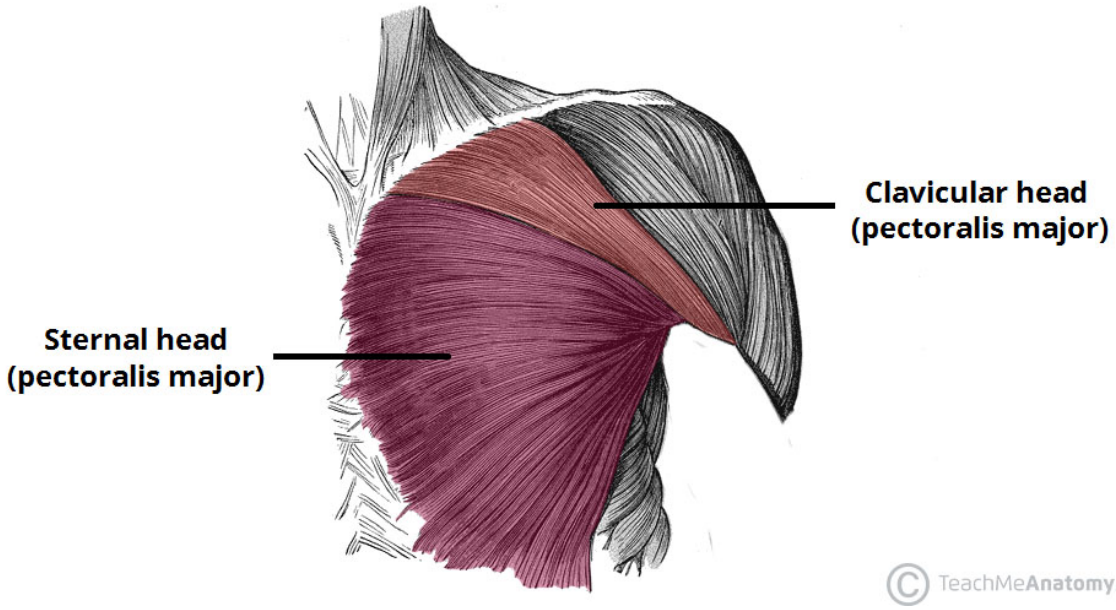


Figure 2.8: Frontal view of the pectoralis major muscle of the left arm. Image taken from: [23]

The infraspinatus is finally shown on Figure 2.9. The infraspinatus is one of the muscles of the rotator cuff. Its main actions are the external rotation of the shoulder and the lateral rotation of the arm. We expect to observe a high activity during the trials where a counter-clockwise force field is applied.

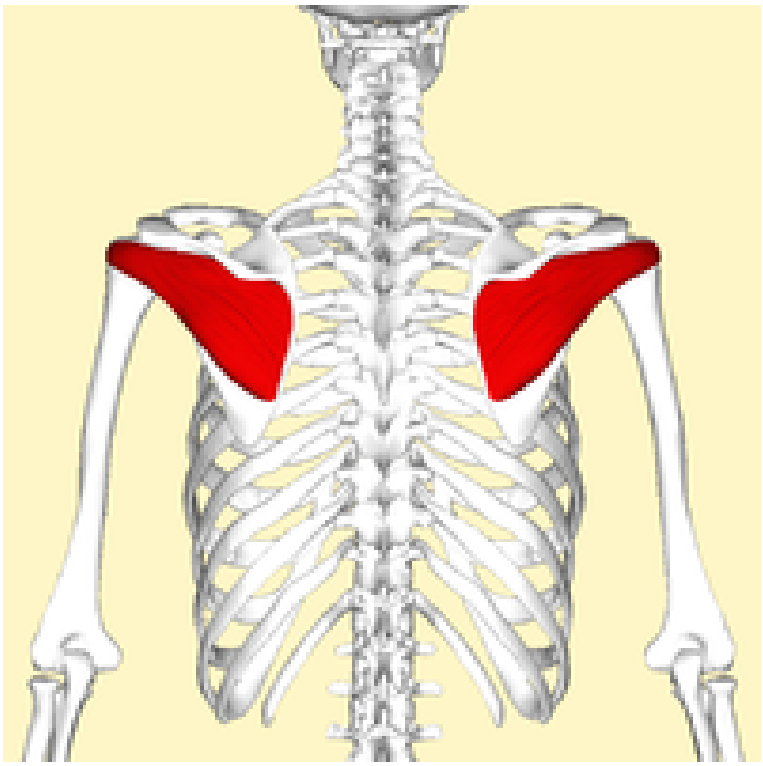

Figure 2.9: Posterior view of the infraspinatus muscles. Image taken from: [24]

**Electrodes**

As explained above, we investigated the activity of 6 muscles. We therefore needed to place 6 electrodes on the participant to record the activity of those muscles, as well as one final reference electrode placed on the lateral malleolus of the ankle.

Figure 2.10 shows the reference electrode. This electrode was pasted on the lateral malleous of the ankle and serves for single use.
Figure 2.11 shows the surface EMG electrode. This electrode is re-usable and was pasted on the skin with a piece of adhesive tape especially designed for it.
The first step before placing the electrodes on the participant was to rub the skin with a piece of cotton soaked with disinfecting alcohol until light abrasion of the skin. This step cleaned the skin and allowed a better contact between the electrode and the skin. We then applied a gel on the two slots of the electrode to enhance the conductivity of the signal.

Figure 2.10: Reference electrode. Image taken from: [25]

Figure 2.11: Surface EMG electrode. Image taken from: [25]

## 2.4 Statistical modelling

We studied the evolution of the overshoot by fitting exponential models to our data, based on standard learning curves.

The presence of significant effects was assessed through paired $t$-tests, repeated-measures ANOVA (rmANOVA) and linear mixed-effects models. The comparison of the models was based on the Bayesian Information Criterion (BIC). The BIC is a criterion used to choose between two

or more models. It is defined as follows:

$$BIC = k\log(n) - 2\log(L(\hat{\Theta})$$

where n is the number of data, k is the number of parameters of the model, $\Theta$ is the set of parameters and $L(\hat{\Theta})$ is the likelihood of the model tested when evaluated at maximum likelihood values of $\Theta$.[26] The lower the BIC, the better the model. Indeed, the BIC increases with the number of parameters used to describe the model and decreases with the likelihood of the model. We performed model comparison to assess if the results obtained through our models captured a real phenomenon in the data or if the results were the consequence of a model that over-fits the data.

The model of EMG activity was collapsed in a 30 ms time interval as a function of the kinetic and kinematic parameters by taking inter-individual variability in addition to differences between first and last few perturbed trials to remove the variability due to learning.

The rmANOVA was performed with the software R, using the package **ez** and the function **ezANOVA**. The linear mixed-effects models were computed with the software R, via the package **nlme** and the function **lme**. The rest of the analysis was performed with the software Matlab.

# Chapter 3

# Results

## 3.1 Analysis of the trajectory

Figure 3.1 shows the evolution of the trajectory for the clockwise trials while Figure 3.2 focuses on the counter-clockwise trials. Each figure depicts the trajectories of the 18 partcipants with comparison to trajectories obtained during the last baseline trial, again for all participants.

Figure 3.1a shows the trajectories of the 18 participants during the first clockwise trial and during a baseline trial. One can see that the force-field trajectories first followed the baseline trajectories, but then quickly deviated as the perturbation was applied. During the first perturbed trial, it also appears that all participants tried to compensate for the perturbation but failed to correctly estimate that compensation and ended up doing an overshoot: the trajectories clearly go beyond the target before finally reaching it. If we now confront those observations with the trajectories obtained during the last clockwise trial depicted in Figure 3.1b, we can see that the overshoot is no longer present. However, it seems that the maximum deviation has not changed much.

Figure 3.2a and Figure 3.2b show the same comparison as above but this time for counter-clockwise trials. The same observations can be made: there is a clear overshoot to the right of the target and this overshoot is almost gone in the trajectories of the last trials. As for the clockwise trials, the maximum deviation does not seem to evolve much between the first and the last perturbed trial.

We just observed that the overshoot present in the first trial has almost disappeared in the last trial for both the clockwise and the counter-clockwise perturbations. It also seems that the maximum deviation remained quite stable between the first and the last trial. We are now going to focus on the evolution of these two parameters across all trials. To do so, for each trial, the mean and the standard deviation of the overshoot and the maximum deviation were computed across all participants.

The obtained results are depicted on Figure 3.3. Figure 3.3a and Figure 3.3b respectively show the results for the clockwise and the counter-clockwise trials. In both cases, the maximum deviation is statistically similar across the trials, as expected. The maximum deviation is approximately equal to 10 cm and 0 cm respectively for clockwise and counter-clockwise trials because the target is located at 5 cm on the x-axis. On the other hand, the overshoot clearly presents a learning behaviour. In both figures, we fitted the means of the overshoots with exponential curves. One can see that it only takes about ten trials to reach a plateau, whether for the clockwise or the counter-clockwise perturbations.

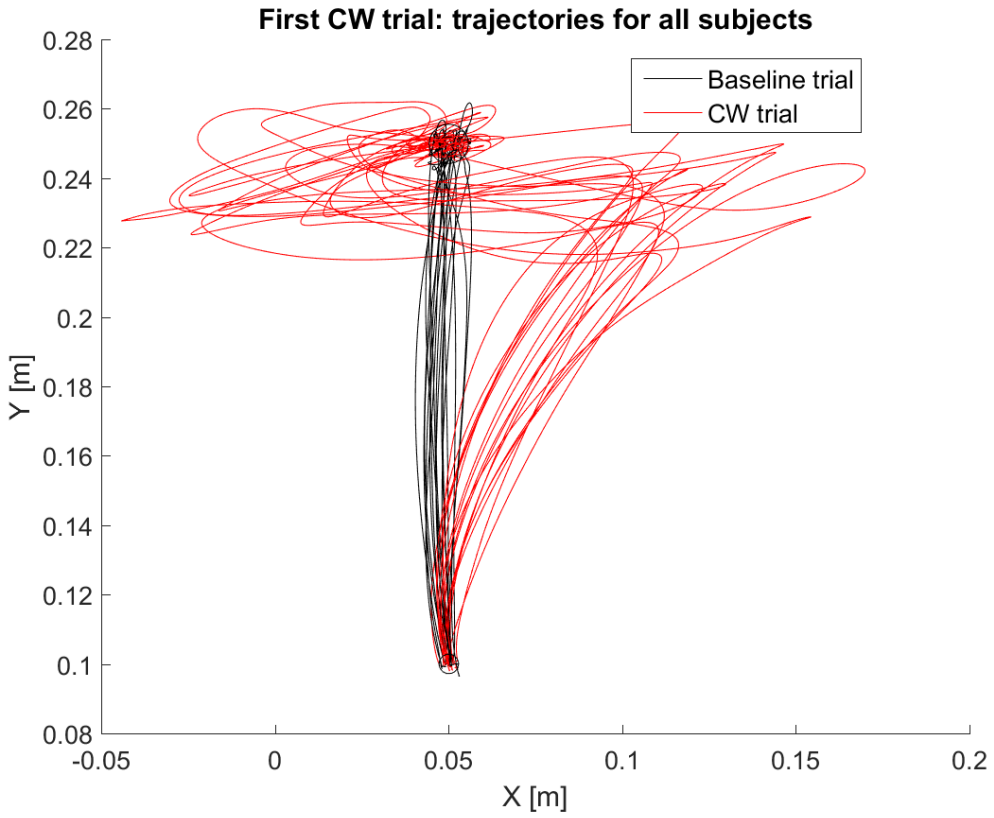


(a)

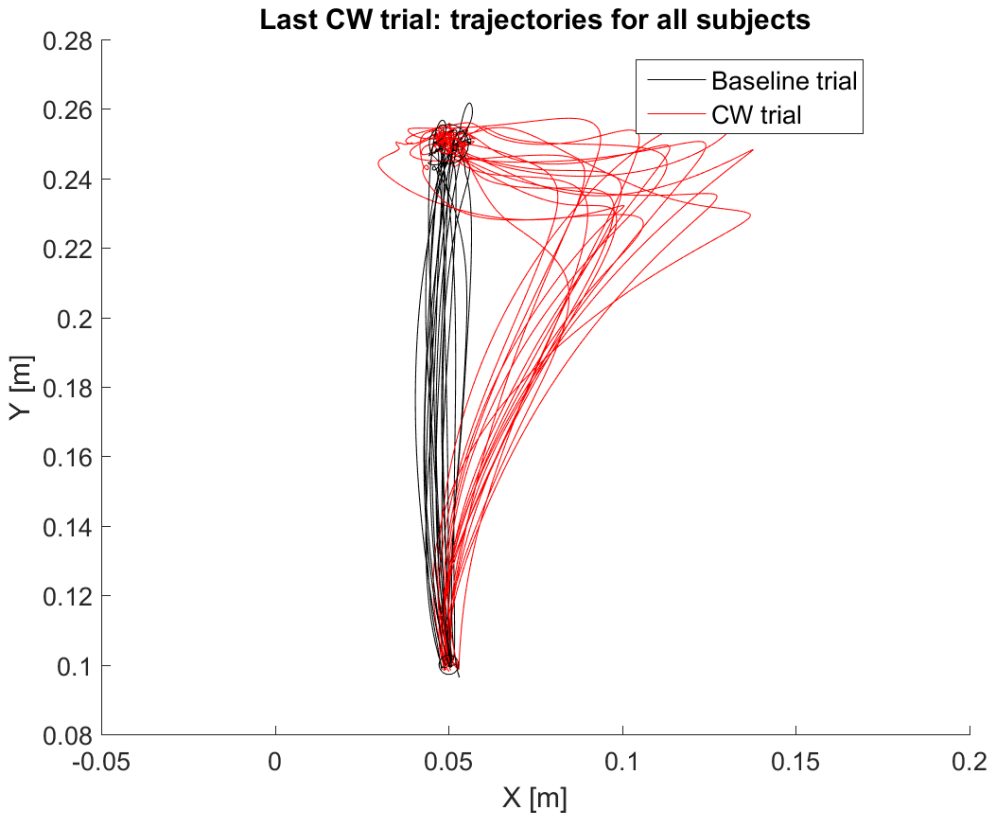


(b)

Figure 3.1: Trajectories of the 18 participants: comparison between last baseline trials (black) and clockwise force-field trials (red). (a) First perturbed trial. (b) Last perturbed trial.

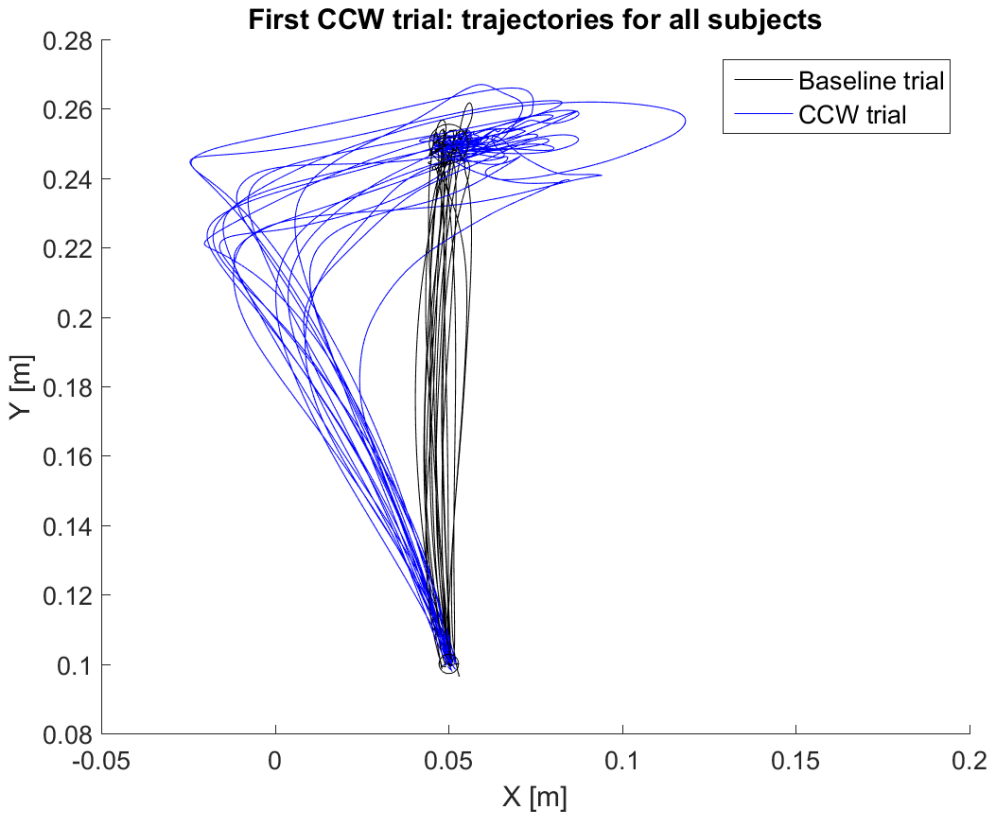


(a)

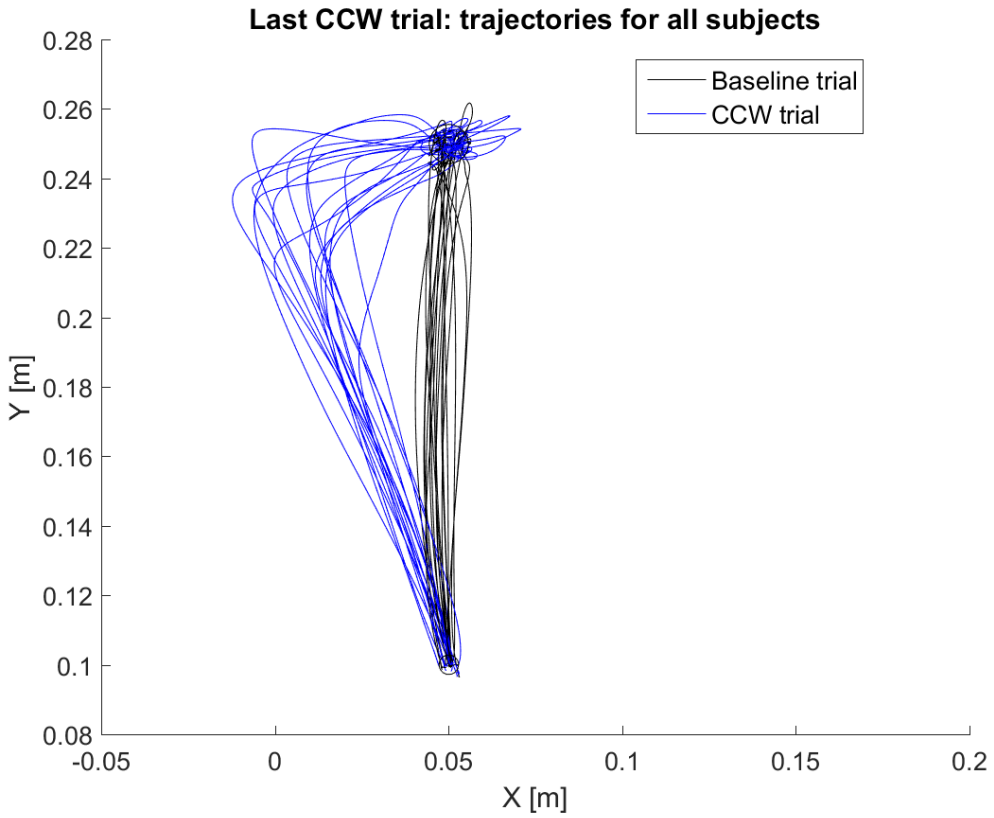


(b)

Figure 3.2: Trajectories of the 18 participants: comparison between last baseline trials (black) and counter-clockwise force-field trials (blue). (a) First perturbed trial. (b) Last perturbed trial.

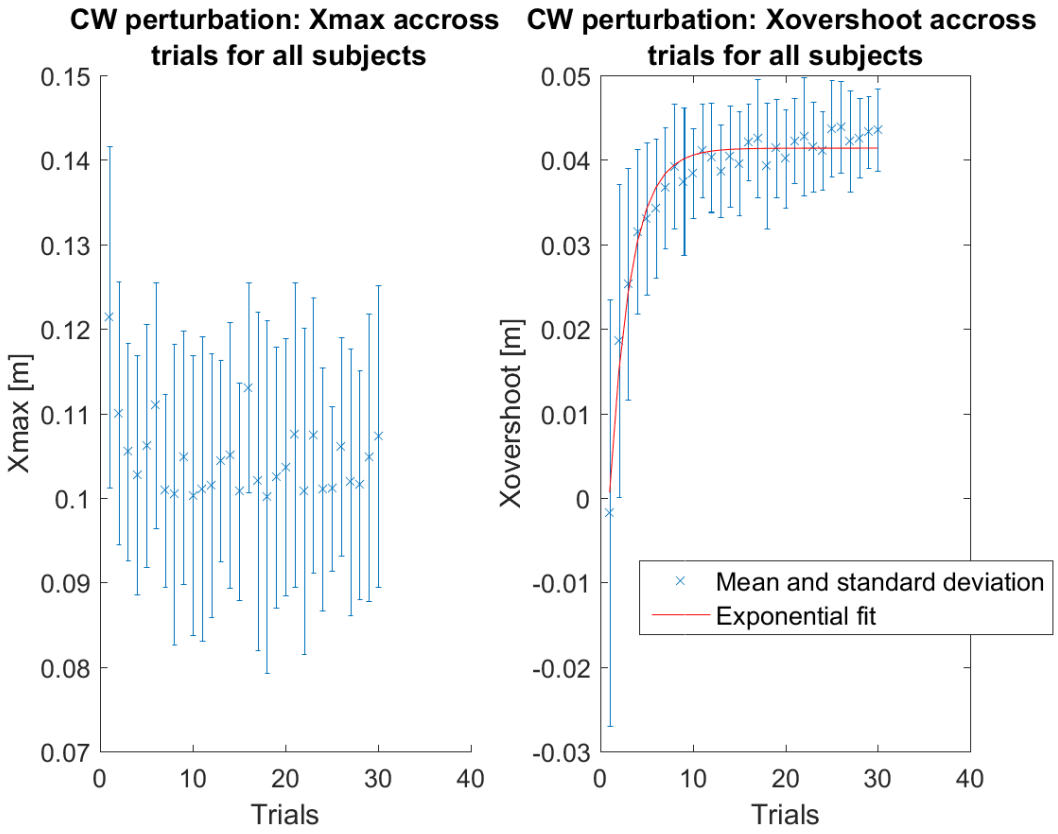


(a)

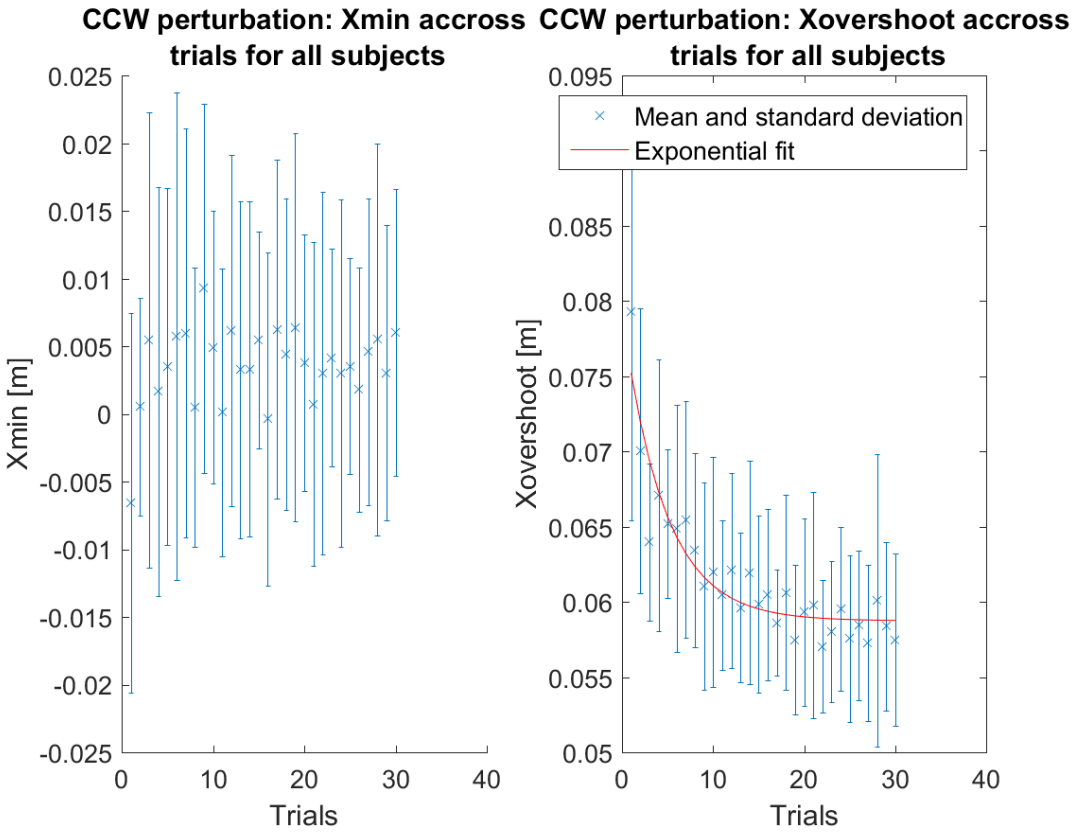


(b) Mean and standard deviation across trials for all participants; left: maximum deviation along the x-axis; right: overshoot along the x-axis. (a) Clockwise perturbation. (b) Counter-clockwise perturbation.

Figure 3.3

## 3.2 Analysis of the force

The analysis of the trajectories leads us to focus on the forces measured at the right handle of the robotic device. To do so, we computed and compared the mean of the forces applied during the first and the last trial across all participants, both for the clockwise and the counter-clockwise perturbations. These curves are depicted in Figure 3.4. The curves are represented in function of time. In both figures, the first second of the graph approximately corresponds to the time at which the participants wait in the starting point for the trial to begin. The last second approximately corresponds to the time at which the participants stabilize their position in the target.

We first analyze the curves of the clockwise perturbation, shown on Figure 3.4a. Since the clockwise force field tried to displace the arm in the +x-direction, the participant fought against this force and therefore applied a force oriented in the opposite direction. Indeed, the resultant of the x-force measured at the handle is first oriented in the -x-direction. After some time, the participant applied a force in the +x-direction: this corresponds to the overshoot. If we compare the curves of the first and the last trial, we can clearly see that the positive peak of the red curve is smaller than the positive peak of the blue curve. This diminution is consistent with the diminution of the overshoot between the first and the last trial. Even though it is less obvious, we can also see that the negative peak of the red curve arises sooner in time than the negative peak of the blue curve. If we now look at the curves of the y-force, we can see that the global pattern remains quite constant between the first and the last trials. The participants tend to push harder in the +y-direction and reach the negative peak sooner in time during the last trial.

The forces of the counter-clockwise perturbation are depicted in Figure 3.4b. In opposition to what we saw above, the participants started by applying a force oriented in the +x-direction to overcome the counter-clockwise perturbation applied in the -x-direction. The negative peak that follows correspond to the overshoot. The diminution of the overshoot between the first and the last trial is obvious in this case. Indeed, we no longer observe a negative peak in the red curve. Participants also applied a bigger force in the +x-direction and the positive peak arises a little bit sooner in time during the last trial. If we now look at the curves of the y-force, we can see that the general pattern of the curve does not change much between the first and the last trial. As for the clockwise perturbation, the participants pushed harder in the +y-direction.

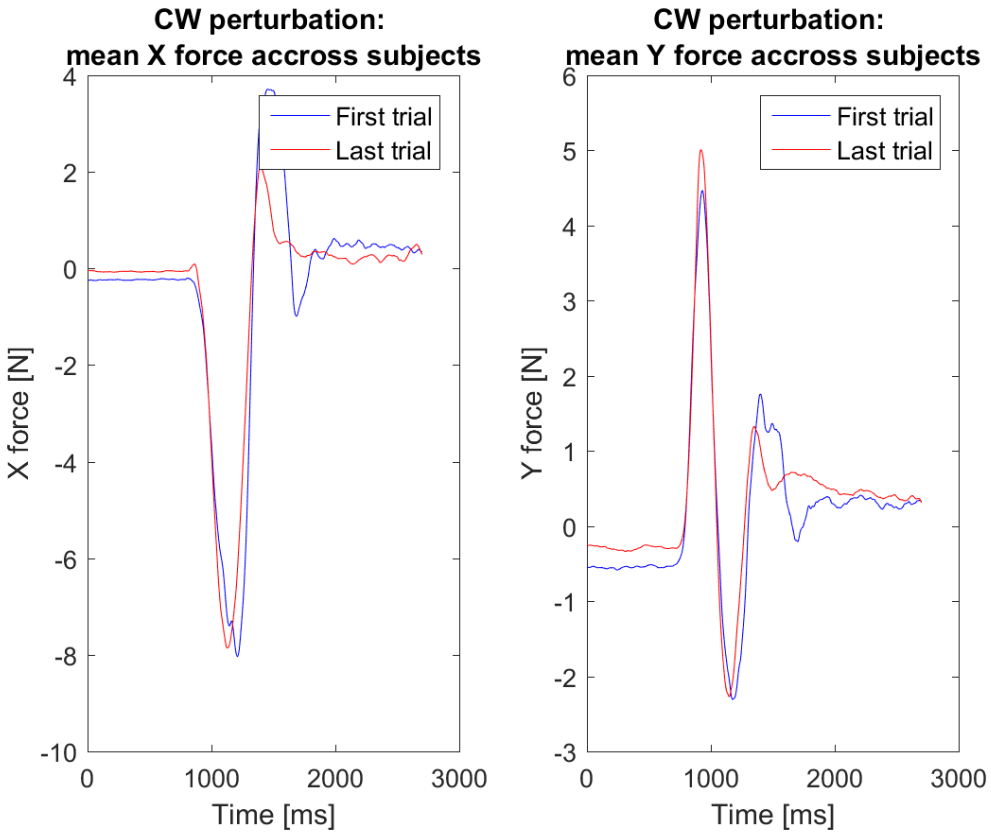


(a)

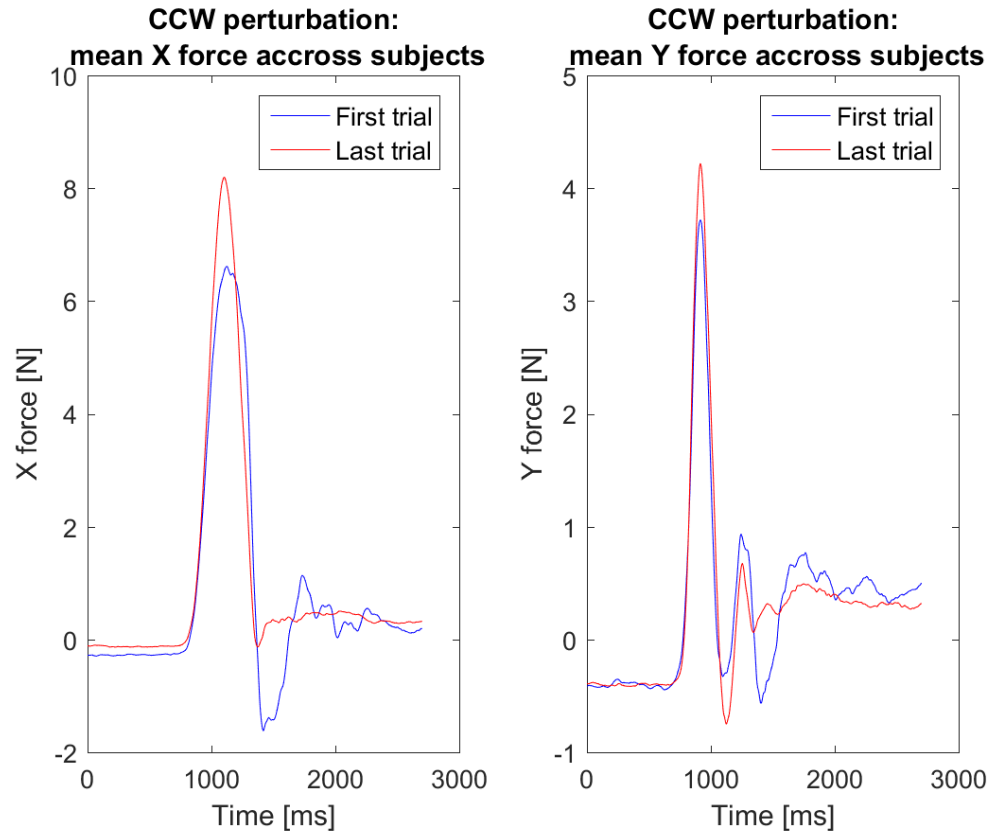


(b)

Figure 3.4: Mean of forces across participantss for the first and the last trial; left: x-force; right: y-force. (a) Clockwise perturbation. (b) Counter-clockwise perturbation.

## 3.3 Analysis of the EMG activity

We just saw that the trajectories performed by the participants and the forces recorded at the handle of the robotic device changed between the first and the last perturbed trials. We are now going to see if those changes also express themselves in the EMG curves. For each muscle and for each perturbation, the EMG curve was obtained by computing a mean across the 18 participants. We are looking for a change in EMG activity between the first and the last perturbed trials. However, EMG data are very noisy, even after filtering. To face that issue, we decided to compute a mean across trials in each participant to obtain the curves corresponding to the behaviour under the first perturbation and the behaviour under the last perturbation. As we saw in the previous results (see Figure 3.3), it appears that the evolution of the overshoot can be fitted by an exponential curve. Therefore the behaviour changes rapidly through the first perturbed trials. For that reason, the curve of the first perturbed trial was obtained by taking the mean of only the two first perturbed trials. We also saw that the overshoot reaches a plateau after about ten perturbed trials. Since the behaviour seems to be stable along the last perturbed trials, it allowed us to compute the curve of the last perturbed trial as the mean of the five last perturbed trials.

The results are depicted in Figures 3.5 and 3.6 respectively for the counter-clockwise perturbation and for the clockwise perturbation. Each sub-figure corresponds to one muscle. The blue curve is the curve of the first perturbation and the red curve is the curve of the last perturbation. As for the analysis of the forces at the handle, the curves are depicted in function of time. For each curve, the first second of the graph approximately corresponds to the time at which the participants wait in the starting point for the trial to begin. The last second approximately corresponds to the time at which the participants stabilize their position in the target.

We observe in both figures that the blue and the red curves can be distinguished for each muscle. As expected, the red curves appear to be less noisy than the blue curves. This makes sense since the blue curves result from the mean of two trials whereas the red curves result from the mean of five trials. One can also observe that for each muscle, there is always a time at which the red curve is clearly located below the blue curve. This stands for the two types of perturbations and this indicates that the intensity of the muscle activity decreases between the first and the last perturbed trials, at least at some point during the last trial. It makes sense to observe that diminution in the activity generated by the muscles, as we saw in Figures 3.4b and 3.4a that the forces recorded at the handle and therefore the forces generated by the participants decreased between the first and the last perturbed trials.

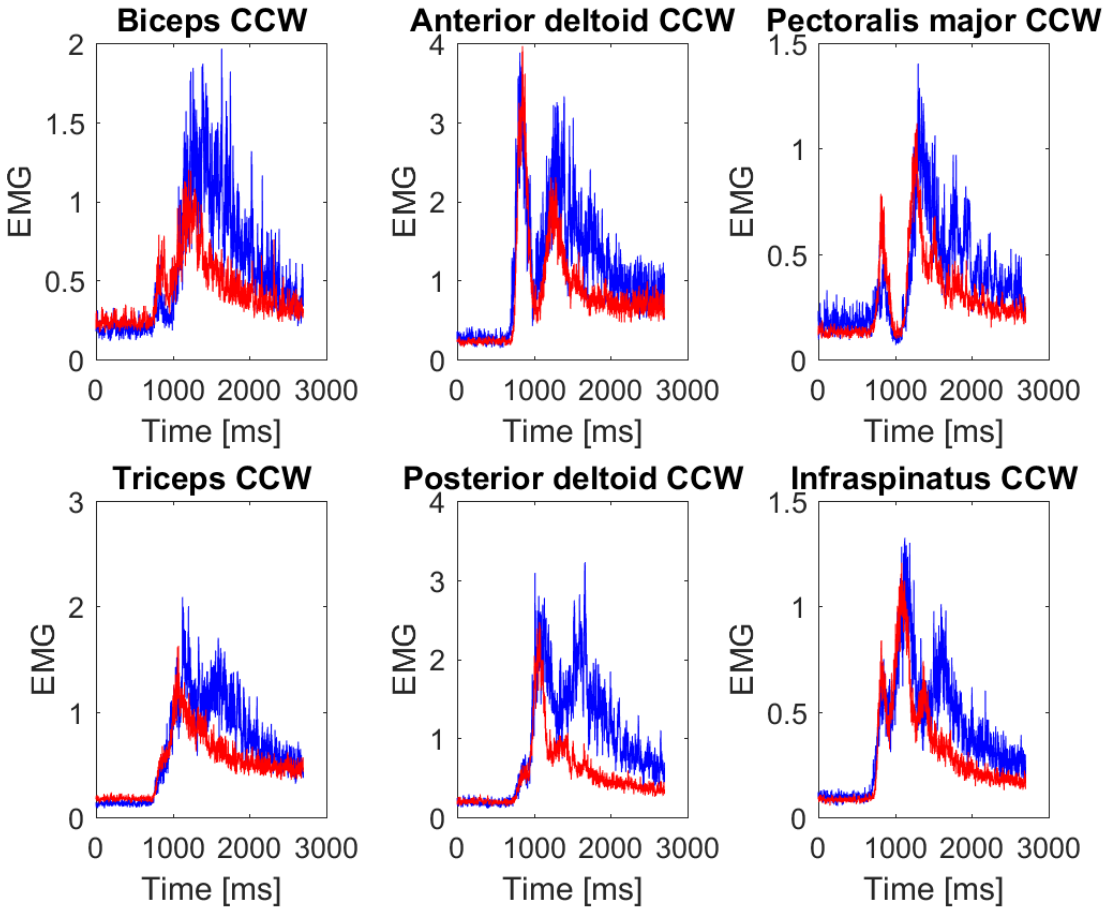


Figure 3.5: EMG activity of the six muscles during counter-clockwise perturbation. Blue: mean of the two first perturbed trials through all participants; red: mean of the last five perturbed trials through all participants.

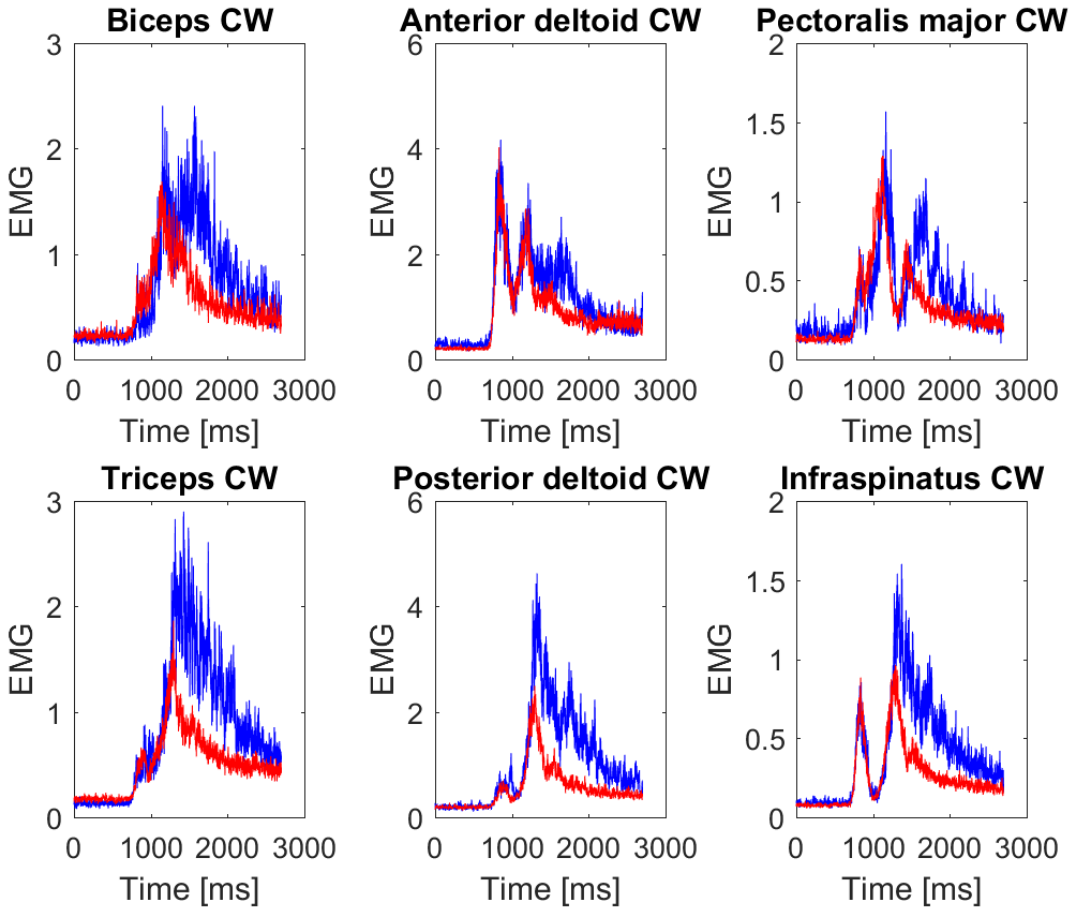


Figure 3.6: EMG activity of the six muscles during clockwise perturbation. Blue: mean of the two first perturbed trials through all participants; red: mean of the last five perturbed trials through all participants.

### 3.3.1 Pectoralis major and infraspinatus

We now focus on the pectoralis major and the infraspinatus muscles. As a remainder, the pectoralis major mainly takes action during the adduction of the arm and the medial rotation of the humerus whereas the infraspinatus main actions are the external rotation of the shoulder and the lateral rotation of the arm. Since one is responsible for the medial rotation of the arm and the other is responsible for its lateral rotation, we expect to observe different behaviours in function of the applied force field. Figure 3.7 shows the last perturbations of those two muscles for both perturbations. One can see that a certain symmetry emerges from those curves. Indeed, the activity of the pectoralis major during a counter-clockwise trial is very similar to the activity of the infraspinatus during a clockwise trial. In the same way, the activity of the pectoralis major during a clockwise trial follows the same shape of the activity of the infraspinatus during a counter-clockwise trial.

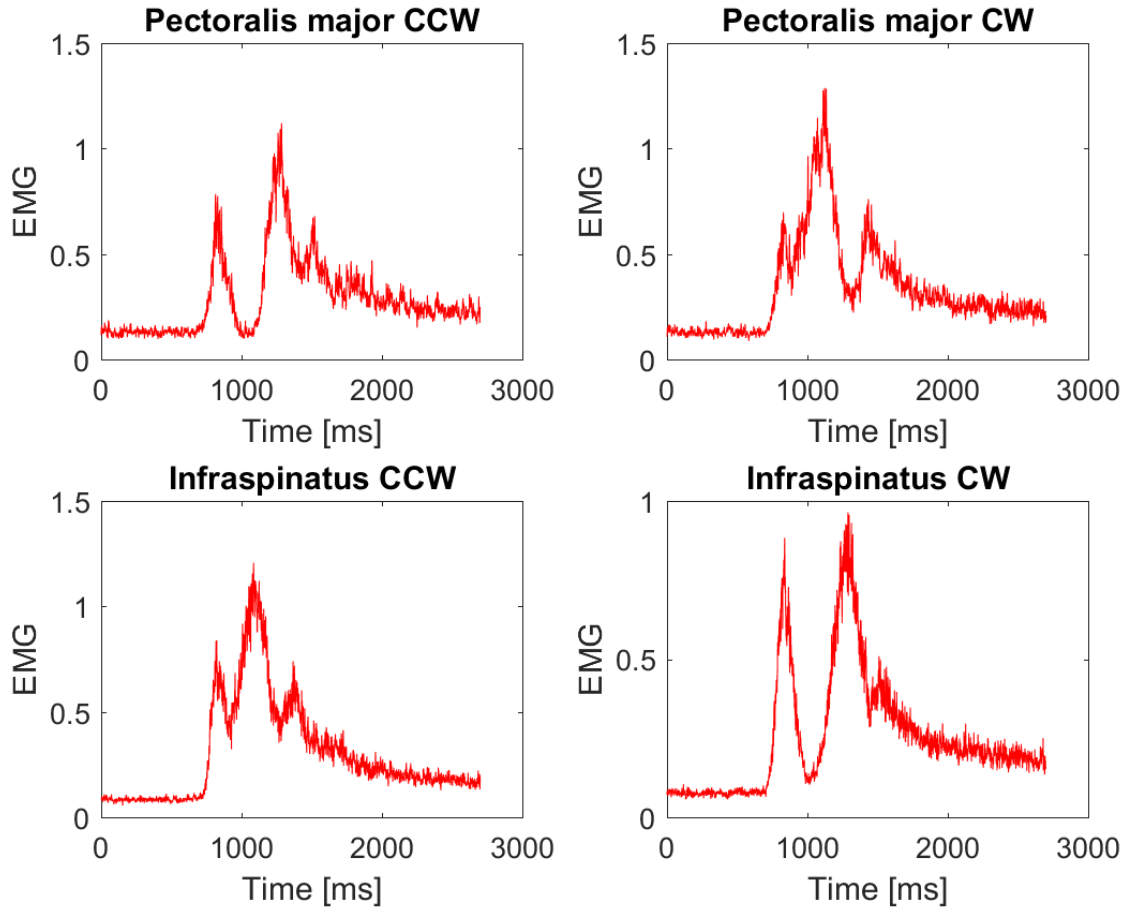


Figure 3.7: Comparison of the mean of the last five perturbed trials through all participants between the pectoralis major and the infraspinatus, during clockwise and counter-clockwise trials.

We analyze here the EMG activity with respect to the perturbation. During a counter-clockwise trial, the force field pushed the arm to the left, closer to the body. Therefore, the participants should first recruit muscles that move the arm away from the body in order to overcome that force field. We then expect to observe an increase in activity in the muscles that move the arm closer to the body, so that the participants can stabilize their hand position inside the target and avoid an overshoot. The reverse situation holds for a clockwise perturbation.

Figure 3.8 shows the comparison of the mean of the last five perturbed trials through all participants between the pectoralis major and the infraspinatus, during clockwise and counter-clockwise trials. In both perturbations, there is a brief co-contraction of the two muscles at the beginning of the movement. However, the expected behaviour described above can be observed for the two perturbations. Indeed, as shown in Figure 3.8a, the infraspinatus was first recruited while the pectoralis major was inhibited. As the end of the trial approached, the two muscles switched their behaviour and the activity of the pectoralis major increased while the one of the infraspinatus decreased. If we finally look at Figure 3.8b, we can see that the peak of activity of the pectoralis major occurred when the activity of the infraspinatus was almost zero. The infraspinatus was then recruited while the activity of the pectoralis major decreased.

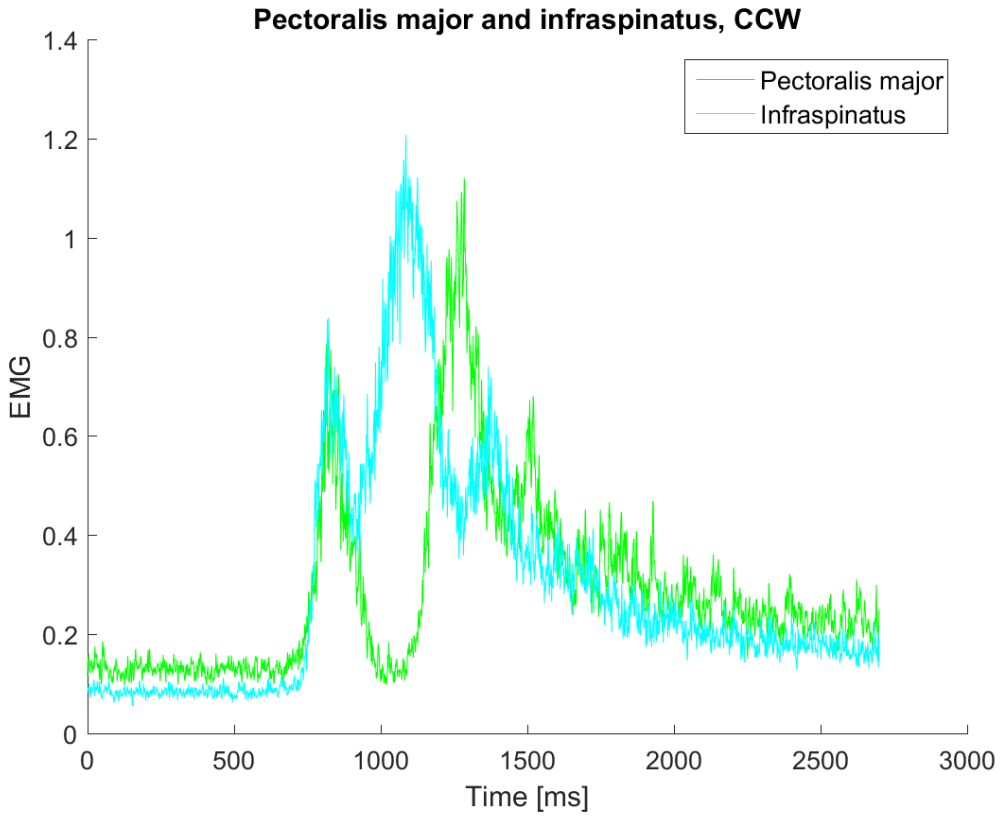


(a)

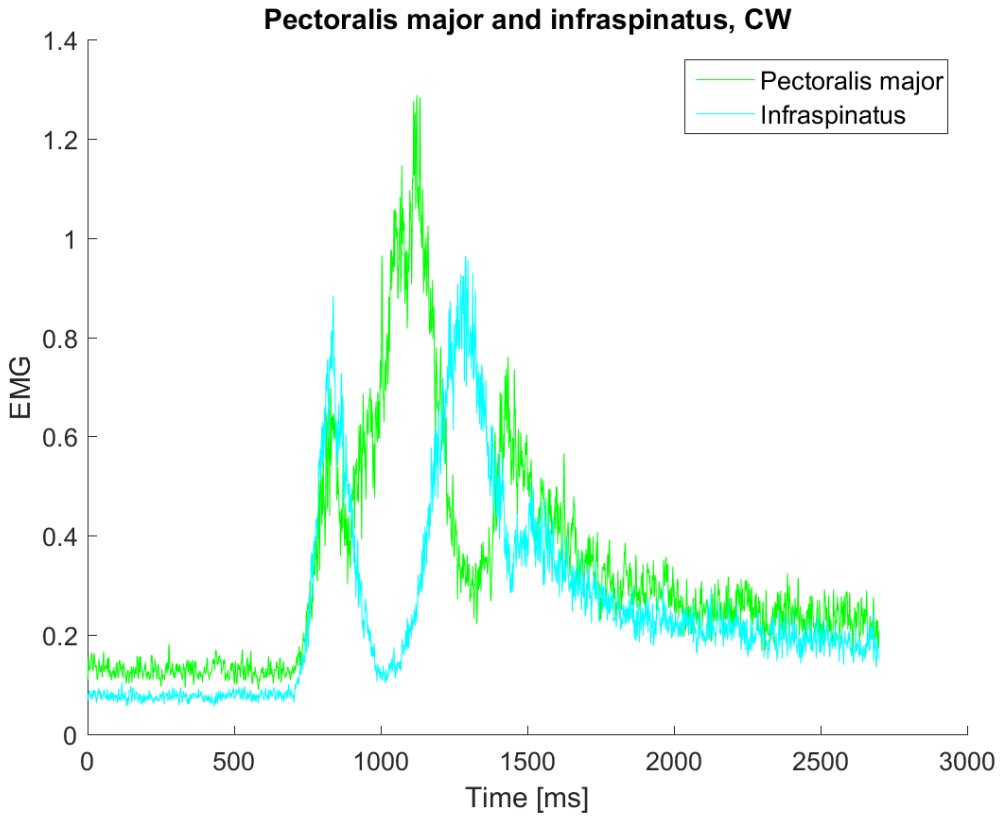


(b)

Figure 3.8: Comparison of the mean of the last five perturbed trials through all participants between the pectoralis major and the infraspinatus. (a) Counter-clockwise perturbation; (b) Clockwise perturbation.

### 3.3.2 Anterior and posterior deltoids

We carry on the analysis by observing in more details the behaviour of the anterior deltoid and the posterior deltoid. As a remainder, the anterior deltoid is responsible for the flexion and the medial rotation of the arm while the posterior deltoid manages the extension and the lateral rotation of the arm. The EMG activity of those two muscles is depicted in Figure 3.9. The curves are the mean of the last five perturbed trials through all participants during counter-clockwise and clockwise trials, respectively shown in Figures 3.9a and 3.9b. We do not observe at first a clear exchange of behaviour between the two muscles as we did above for the pectoralis major and the infraspinatus. However, if we look at the counter-clockwise curves, we can see that there is a coordination between the two muscles. Indeed, when the anterior deltoid was active, the posterior deltoid was inhibited and vice versa. This makes sense since the anterior and posterior deltoids form an agonist/antagonist pair of muscles. This last behaviour is less obvious during the clockwise trials.

If we now focus on the posterior deltoid, we can see that its behaviour during the clockwise perturbation differed from its behaviour during the counter-clockwise perturbation. Indeed, its main activity seems to occur later in the trial for a clockwise perturbation. During a clockwise perturbation, the participant had to overcome the force field which displaced the arm to the right, away from the body. This means that we expect to first observe a higher activity in the muscles responsible for the movement that brings the arm closer to the body, in this case, the anterior deltoid. The posterior deltoid was therefore at first inhibited. It activated itself towards the end of the movement, when the participant must stabilize its hand position in the target while avoiding an overshoot. On the contrary, in a counter-clockwise trial, the posterior deltoid should be recruited quicker in order to counteract the perturbation and to move the arm away from the body.

If we finally look at the anterior deltoid, we expect to observe an opposite behaviour than the one of the posterior deltoid. However, one can see that there is a first peak of activity, very similar no matter the type of perturbation. This peak of activity was actually present in undisturbed trials and was thus not specific to a particular perturbation. If we now focus on the activity of the anterior deltoid after the first peak, we can see that as expected, its second peak of activity occurred after the peak of activity of the posterior deltoid for the counter-clockwise trial and reversely for the clockwise trial. In other words, if we ignore the first peak of activity of the anterior deltoid which is not specific to the perturbation, a certain symmetry emerges between the EMG curves of the two muscles, in the same way that the one observed between the pectoralis major and the infraspinatus.

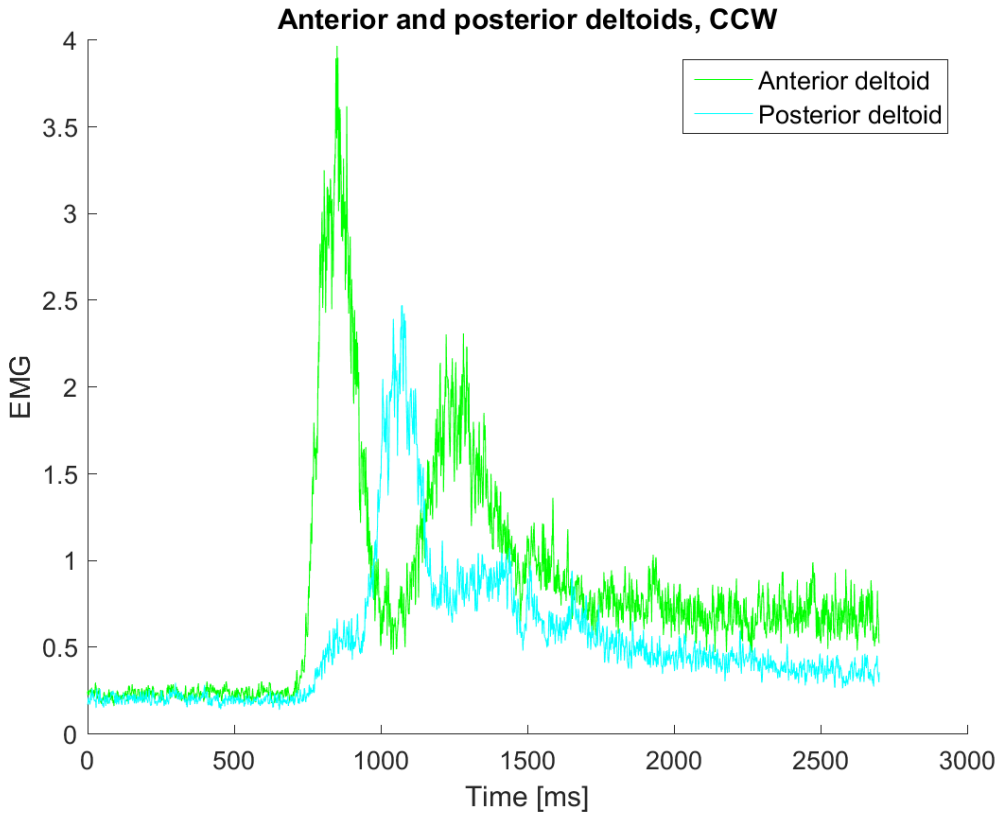


(a)

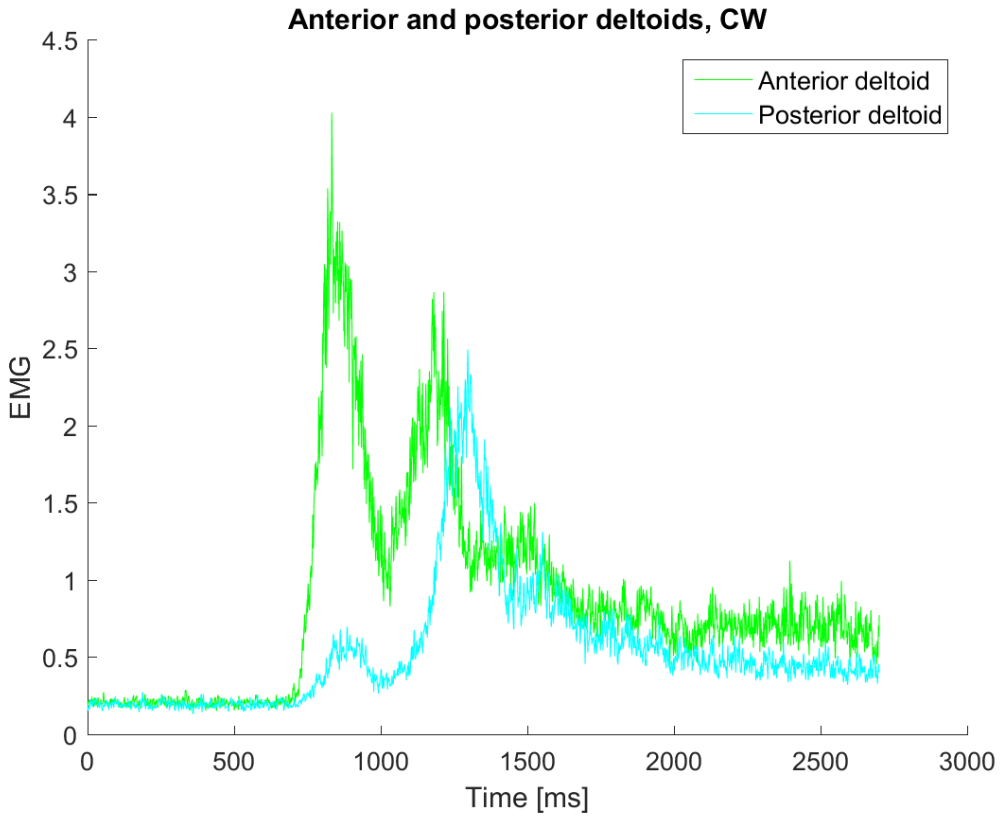


(b)

Figure 3.9: Comparison of the mean of the last five perturbed trials through all participants between the anterior deltoid and the posterior deltoid. (a) Counter-clockwise perturbation; (b) Clockwise perturbation.

### 3.3.3 Biceps and triceps

Figures 3.10 and 3.11 finally highlight the activity of the biceps and the triceps during both perturbations. As a remainder, the biceps is mainly responsible for the flexion of the forearm on the arm while the triceps manages its extension. The biceps and the triceps also form a pair of agonist/antonagonist muscles. During a counter-clockwise trial, we expect the triceps to be recruited first since the force field brought the arm closer to the body and therefore the participants needed to extend their forearm in order to reach the target. On the contrary, the biceps should contract first during a clockwise perturbation since a flexion of the forearm is necessary to correct for the position of the hand.

If we look closely at Figure 3.10, we can see that as for the pectoralis major and the infraspinatus, the muscles seem to switch their behaviour when the perturbation changes. The symmetry is less obvious in this case, first because the curves of the biceps are more noisy than the curves of the triceps; secondly because the four curves are all quite similar.

We finally focus on Figure 3.11 and we confirm our expectations: the triceps contracted first during counter-clockwise trials while the peak of activity of the biceps was the first to occur during clockwise trials.

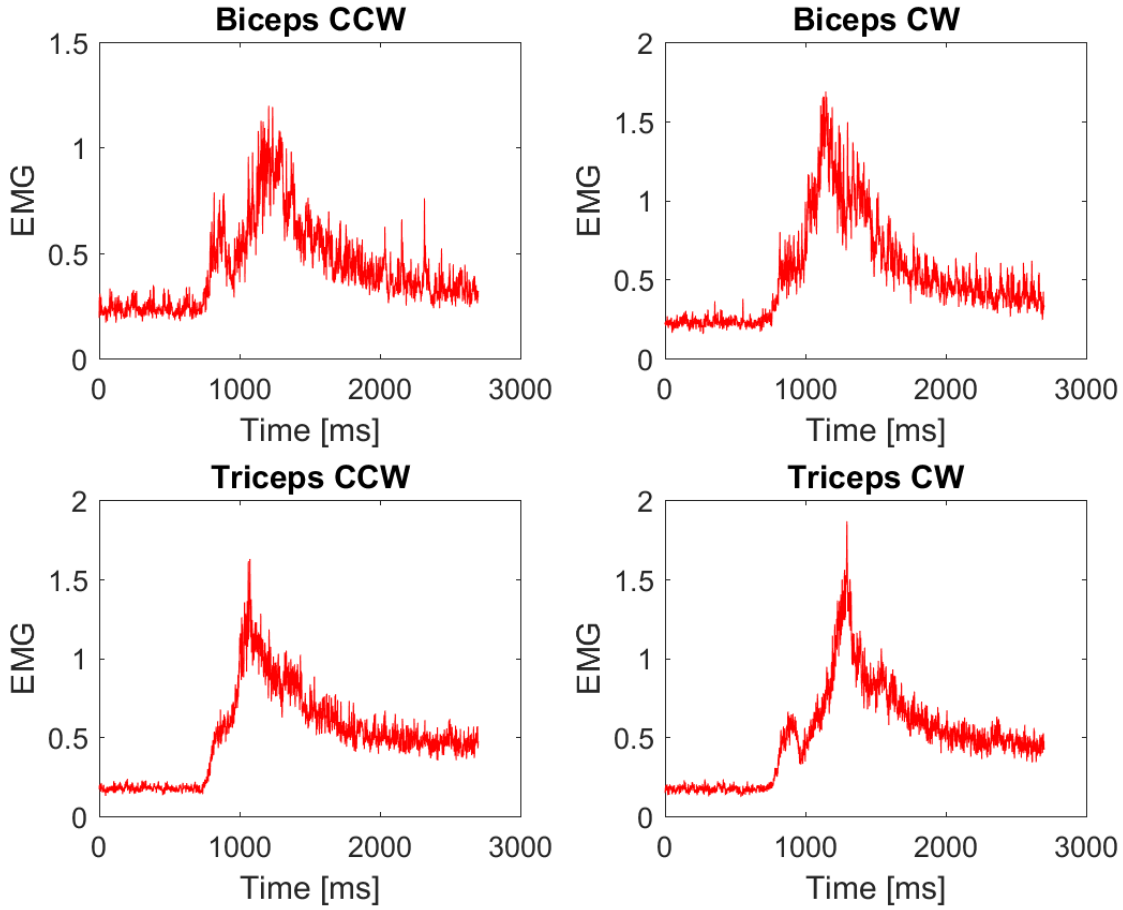


Figure 3.10: Comparison of the mean of the last five perturbed trials through all participants between the biceps and the triceps, during clockwise and counter-clockwise trials.

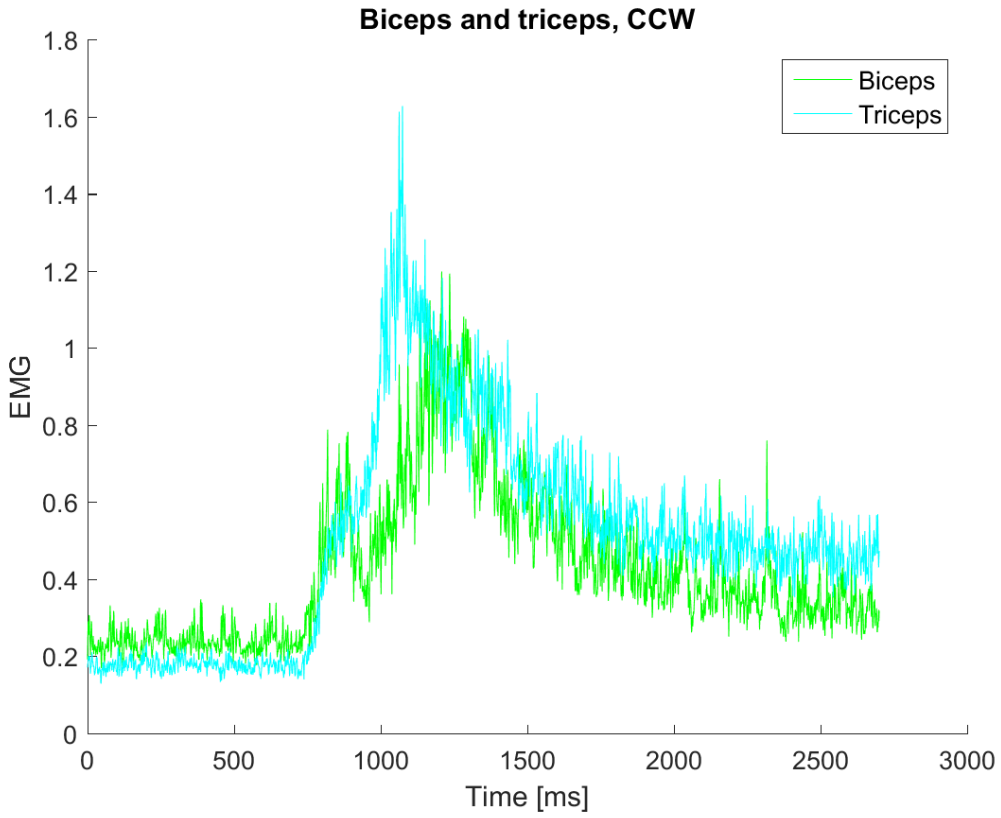


(a)

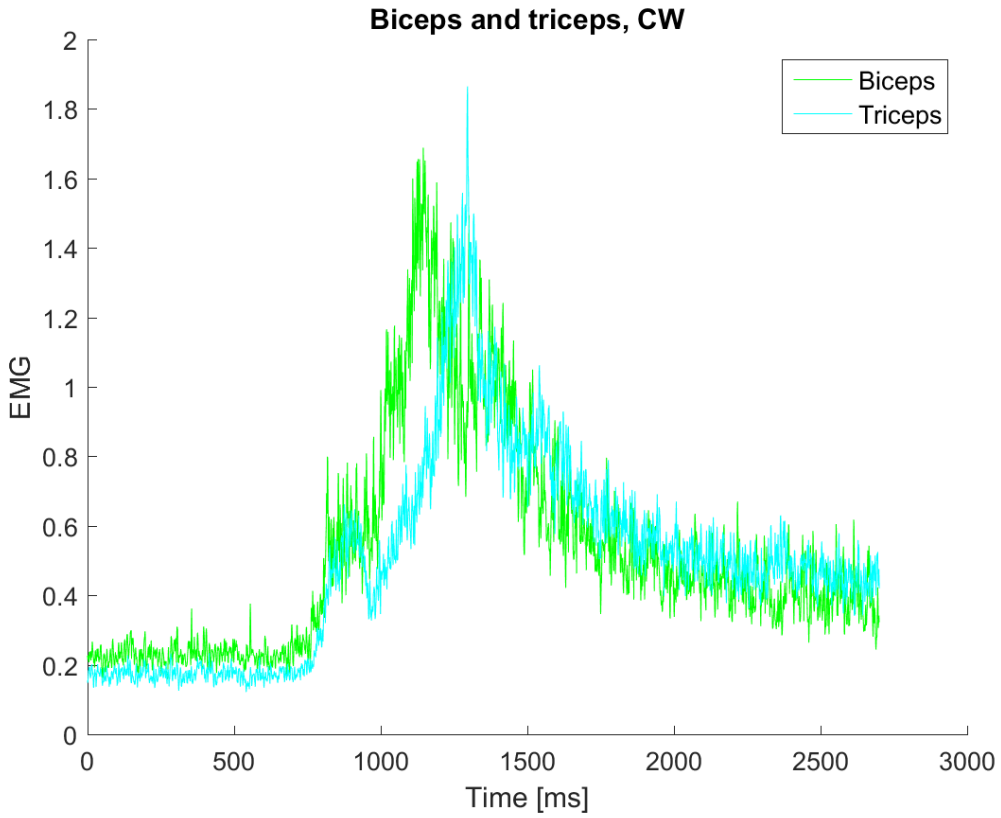


(b)

Figure 3.11: Comparison of the mean of the last five perturbed trials through all participants between the biceps and the triceps. (a) Counter-clockwise perturbation; (b) Clockwise perturbation.

### 3.3.4 Differences in EMG activities and critical times

We previously saw in Figures 3.5 and 3.6 that the EMG curves of the first and last trials could be distinguished for each muscle. What we want to do next is to objectify this difference. To do so, we follow the next steps, for each muscle and for each perturbation:

1. We computed two EMG curves for each participant: the mean of the first two perturbed trials and the mean of the last five perturbed trials. We therefore obtained 18 curves of each category.

2. We performed a temporal mean on the previous curves every 30 time steps. Each value of the curve is now a mean over 30 ms of the initial EMG curves. This allowed to smooth the signal.

3. We computed a paired $t$-test at each time step between the 18 values of the curves of the first trials and the 18 values of the curves of the last trials. We then obtained a vector of p-values which objectify the difference between the curves of the first and the last trials at each time step.

4. We visualized the results: we plotted the logarithm of the p-values in function of time. We also plotted a significant threshold at $\log(0.05)$.

The obtained results are depicted in Figures 3.12 and 3.13, respectively for counter-clockwise and clockwise trials. Now that we have obtained the graphs of the p-values in function of time, we can see at what time these curves drop down below the significant threshold. For each muscle and for each perturbation, this time corresponds to the moment at which the behaviour of the participant during the first perturbed trials significantly differs from its behaviour during the last perturbed trials. From now on, this time will be called the critical time. One can see that the curves are quite noisy despite the temporal mean applied on the signals. This noise causes the signals to oscillate a lot and therefore the curves drop down below the significant threshold more than once. For that reason, the acquisition of the critical times was made through a visual analysis of the signals, by keeping in mind the behaviour of the participants depicted in Figures 3.5 and 3.6. The green crosses indicate the critical times for each muscle during counter-clockwise and clockwise trials, respectively in Figures 3.12 and 3.13. The horizontal red bar corresponds to the significant threshold, fixed at $\log(0.05)$. Table 3.1 clusters the critical times for each muscle and each perturbation, expressed in ms. Those critical times are also displayed on the EMG activity of the six muscles, for both perturbations on Figures 3.14 and 3.15 to better visualize the accurate moment at which the behaviour of the participant between the first and the last perturbed trials significantly changed. A final way to visualize that change is depicted in Figure 3.16, where the critical times for each muscle is highlighted on the mean trajectories of the last perturbed trials across participants for both perturbations. One can see that the change in the EMG curves occurred very late in the trial for the anterior deltoid and the pectoralis major as well as for the biceps for clockwise perturbation. For the other muscles, the critical times occurred when the trajectory approximately reached its maximum deviation.

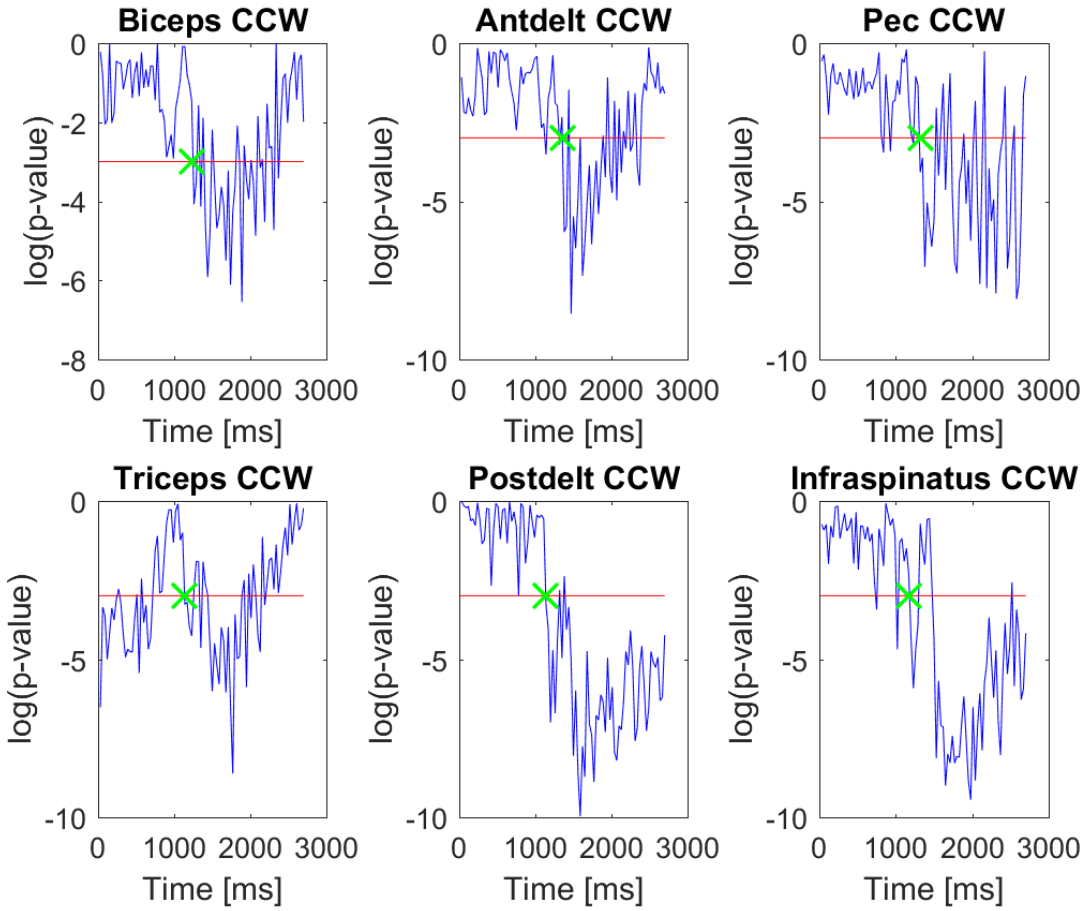


Figure 3.12: Results of the paired $t$-test between the EMG curves of the first and the last counter-clockwise trials. Blue: log(p-values); Red: threshold at log(0.05); Green: critical times.

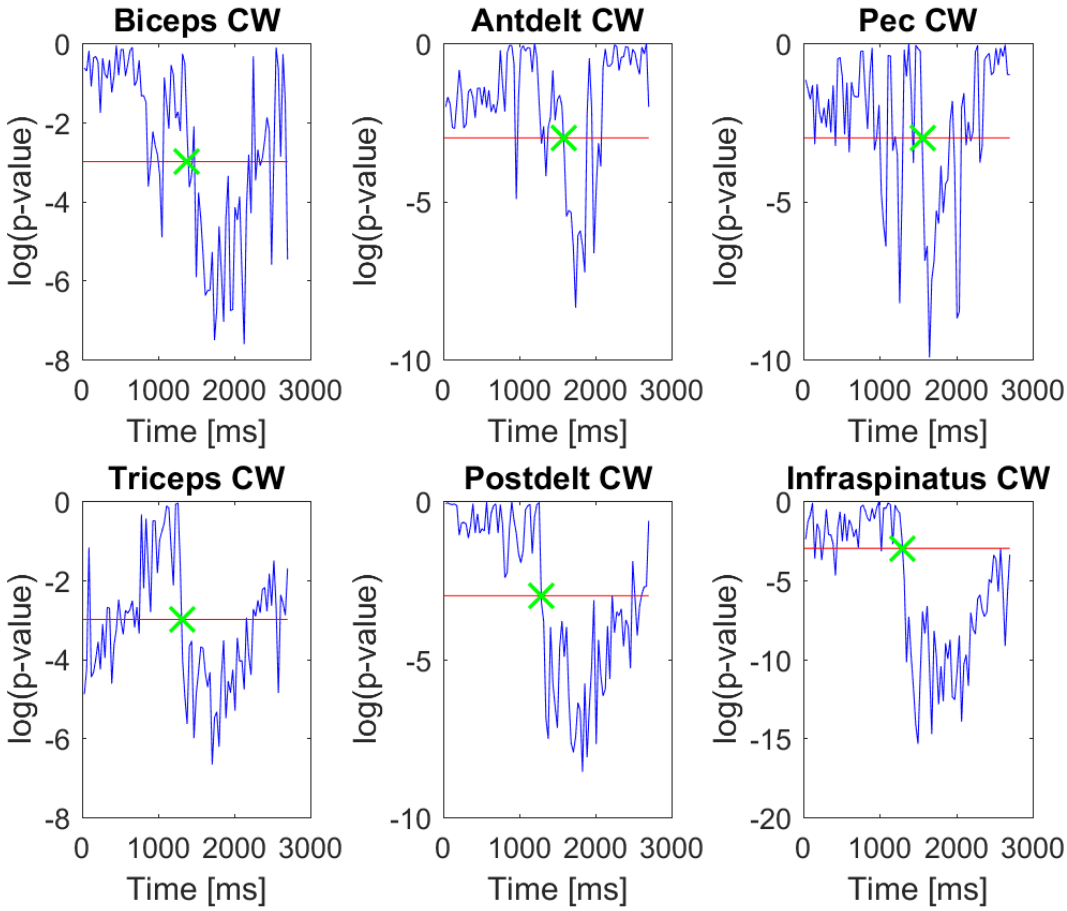


Figure 3.13: Results of the paired $t$-test between the EMG curves of the first and the last clockwise trials. Blue: log(p-values); Red: threshold at log(0.05); Green: critical times.

| Muscle | CCW | CW |
|---|---|---|
| **Biceps** | 1230 | 1380 |
| **Triceps** | 1140 | 1320 |
| **Anterior deltoid** | 1360 | 1590 |
| **Posterior deltoid** | 1140 | 1290 |
| **Pectoralis major** | 1320 | 1560 |
| **Infraspinatus** | 1470 | 1290 |

Table 3.1: Critical times [ms], for each muscle and each perturbation.

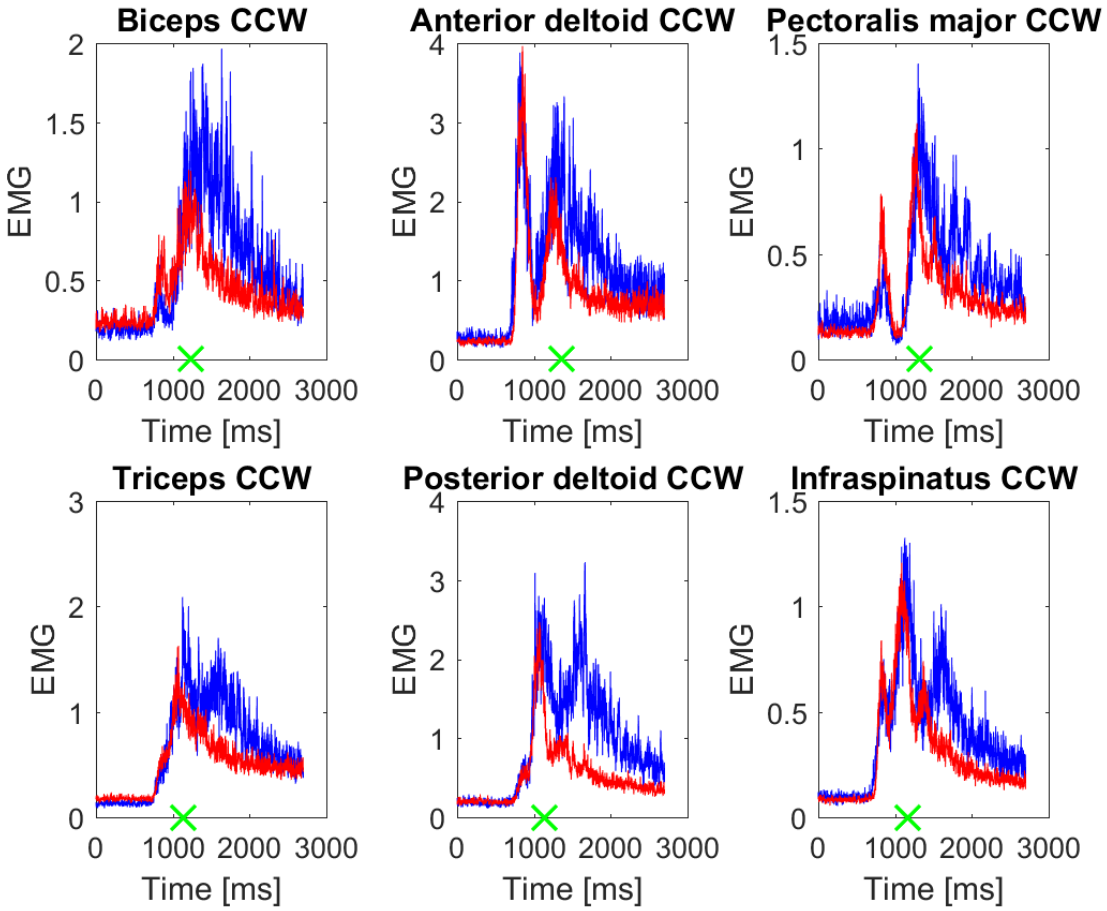


Figure 3.14: EMG activity of the six muscles during counter-clockwise perturbation. Blue: mean of the two first perturbed trials through all participants; red: mean of the last five perturbed trials through all participants; green: critical times.

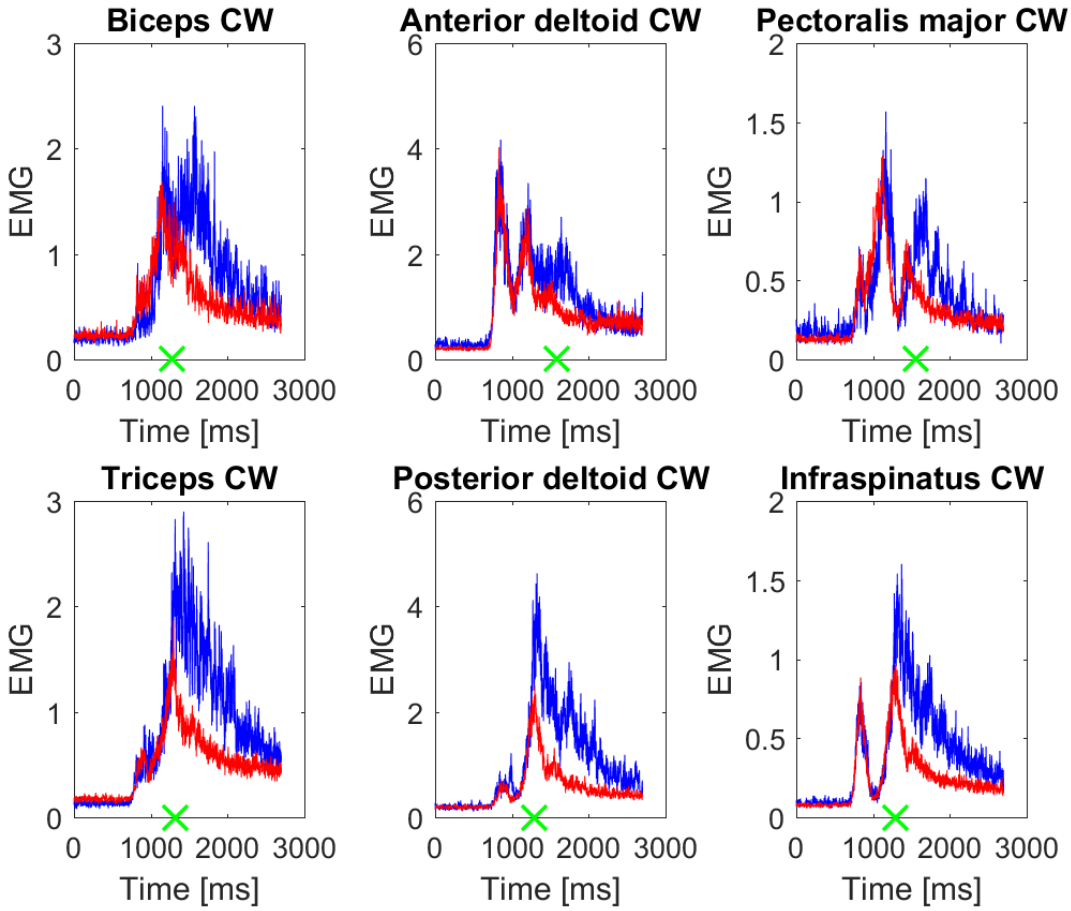


Figure 3.15: EMG activity of the six muscles during clockwise perturbation. Blue: mean of the two first perturbed trials through all participants; red: mean of the last five perturbed trials through all participants; green: critical times

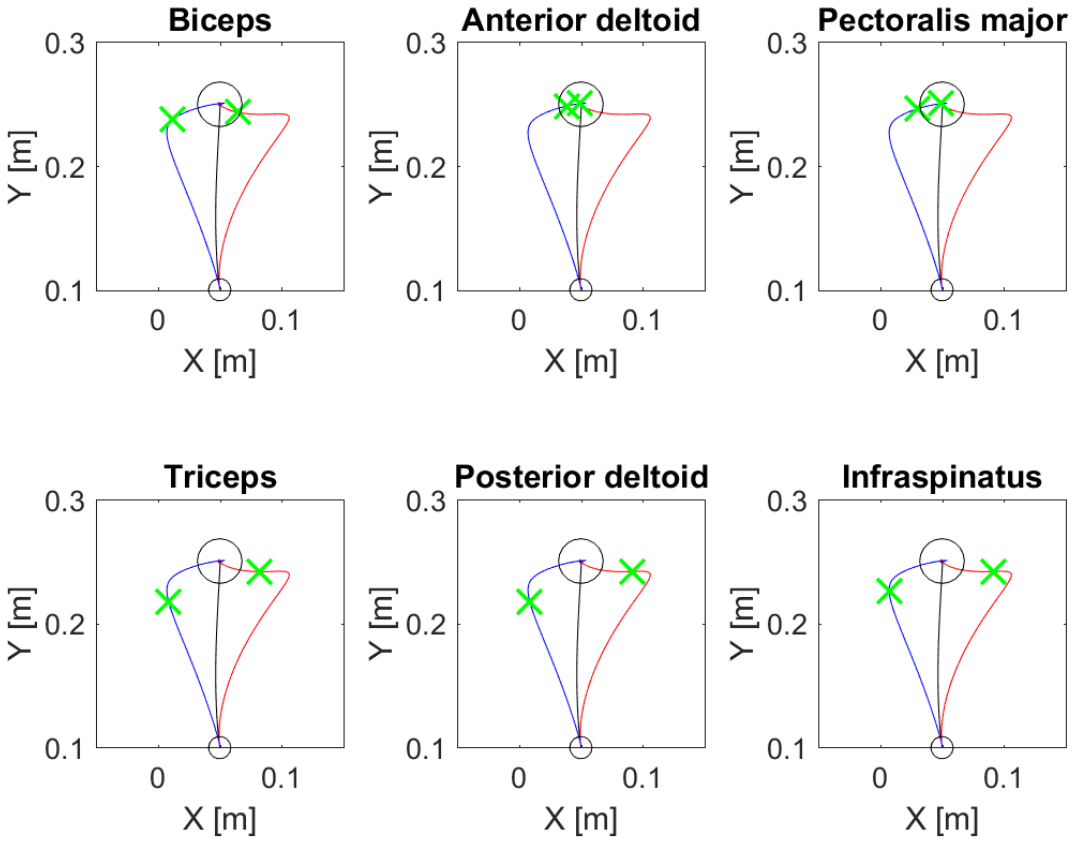


Figure 3.16: Mean trajectories of the last perturbed trials across participants. Blue: counter-clockwise; red: clockwise. The spots of the trajectory corresponding to the critical times are depicted by green crosses.

The next step of the analysis is to situate the critical times with respect to the beginning of the movement. First of all, the beginning of the movement during a trial is defined as the time at which the y-coordinate of the hand's position became strictly greater than 10.6 cm, that is when the position's cursor of the right hand of the participant left the starting point. From now on, this time will be called the starting time. For each participant, starting times were computed for every performed trial (baseline, with a counter-clockwise perturbation and with a clockwise perturbation). We thus obtained a distribution of starting times per participant, composed of 360 (6 blocks of 60 trials each) scalar values.

Figure 3.17 shows the superposition of the 18 starting times distributions, as well as the critical times indicated by vertical lines (red for counter-clockwise, green for clockwise) for each muscle. The main part of the global distribution is centered around 900 ms, that is 100 ms before the reference time on which all signals were aligned. Some values of the histogram are located way later in time: this critical times correspond to missed trials due to a moment of distraction of the participants. Based on the critical times and the distribution of the starting times, we evaluated that the EMG changes during the movement correlated with the improvement of reach control occurred after 375 ms on average after the beginning of the movement.

We then focus on the critical times. As a remainder, those times correspond to the moments during the trial at which a significance difference between the EMG curves of the first and the

last perturbed trials was observed. The first observation that we can make is that the critical times of the counter-clockwise trials occurred all sooner than the critical times of the clockwise trials. We can also see that for each perturbation, the critical times of the triceps, the posterior deltoid and the infraspinatus occurred sooner than the critical times of the biceps, the anterior deltoid and the pectoralis major.

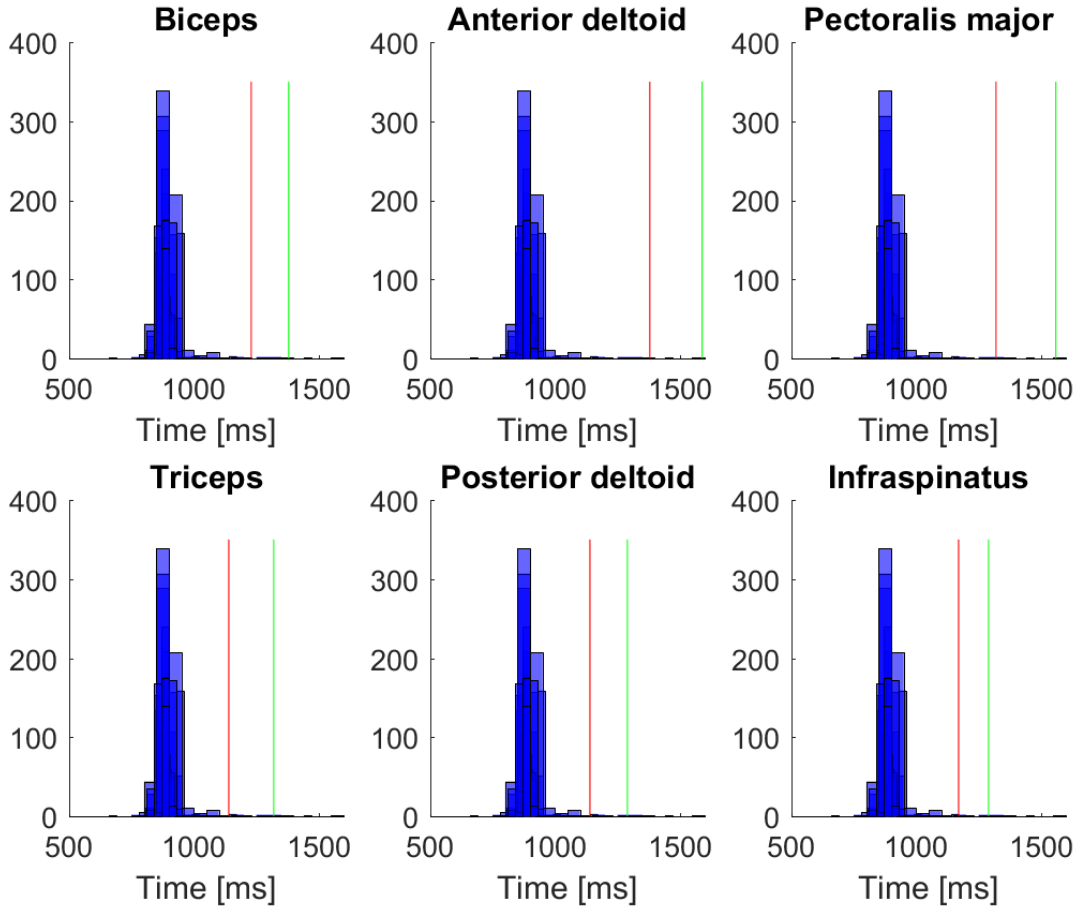


Figure 3.17: Starting times and critical times for each muscle. Blue: distributions of starting times for all participants; red: critical times for a counter-clockwise perturbation; green: critical times for a clockwise perturbation.

### 3.3.5 Statistical analysis

We are now going to perform statistical analysis to:

1. Objectify the significant difference between the EMG curves of the first and the last perturbed trials.
2. See if the cause of that difference can be explained by the kinematics variables of the movement.

We first objectified the significant difference between the EMG curves of the first and the last perturbed trials, in order to confirm the previous observations that we made based on the computation of the p-values of the paired $t$-test. The main idea is to investigate whether or not the type of perturbation (counter-clockwise or clockwise) can predict the difference observed in the EMG curves. To do so, we firstly re-arranged the data in a table: we did that for each muscle

and for each perturbation. The table is made of three columns. The first column contains the ID of the participants, going from 1 to 18. The second one is filled with scalars either equal to one or to two. The scalar one corresponds to a first perturbed trial whereas the scalar two stands for a last perturbed trial. As for the previous analysis, we will look at the first two and the last five perturbed trials for each participant. The third column is also filled with scalars, corresponding to the temporal mean EMG activity, taken over 30 ms after the respective critical time of the muscle. Table 3.2 shows the 14 first lines of such a table. Since there are 18 participants, a full table is made of 126 lines.

| **Participants** | **Trial** | **EMG** |
|---|---|---|
| 1 | 1 | $EMG_1$ |
| 1 | 1 | $EMG_2$ |
| 1 | 2 | $EMG_3$ |
| 1 | 2 | $EMG_4$ |
| 1 | 2 | $EMG_5$ |
| 1 | 2 | $EMG_6$ |
| 1 | 2 | $EMG_7$ |
| 2 | 1 | $EMG_8$ |
| 2 | 1 | $EMG_9$ |
| 2 | 2 | $EMG_{10}$ |
| 2 | 2 | $EMG_{11}$ |
| 2 | 2 | $EMG_{12}$ |
| 2 | 2 | $EMG_{13}$ |
| 2 | 2 | $EMG_{14}$ |

Table 3.2: Example of the re-organization of the data: 14 first lines of the table.

We performed rm-ANOVA on the data with the following settings: the column Participants contains the variable specifying the identifier. The column Trial contains the independent variable, also called the within-participants factor. This factor has two levels: first perturbed trial or last perturbed trial, respectively designed by 1 or 2. Finally, the column EMG is the dependent variable. Table 3.3 summarizes the p-values of the rm-ANOVA performed for each muscle and for each perturbation. As one can see, all p-values are smaller than the significant threshold fixed at $p = 0.05$, meaning that the type of trial (first or last) predicts the difference observed in the EMG curves between the first and the last perturbed trials.

| **Muscle** | **CCW** | **CW** |
|---|---|---|
| Biceps | 0.01568158* | 0.0261111* |
| Triceps | 0.03918893* | 0.007302602* |
| Anterior deltoid | 0.002599674* | 0.004012161* |
| Posterior deltoid | 0.01748072* | 0.02352334* |
| Pectoralis major | 0.02564251* | 0.001107742* |
| Infraspinatus | 0.01102595* | 0.008231141* |

Table 3.3: P-values of the rm-ANOVA. *: $<$ p $= 0.05$

Now that we have objectified the difference between the EMG curves, we want to understand the cause of that difference. A possible explanation is that the kinematics of the movement influences the EMG activity of the participant. To explore that possibility, we had to re-arrange the data in a table: we did that for each muscle and for each perturbation. The first three columns of the table are the same as in the table created to perform the rm-ANOVA. We had

to add four columns to this table, respectively corresponding to the x-position, the y-position, the x-speed and the y-speed of the hand. Table 3.4 shows the first 14 lines of such a table. All kinematics values were taken 30 ms before the critical time, i.e. 30 ms before the EMG curves started to significantly differ from each other.

| **Participants** | **Trial** | **EMG** | **X-position** | **Y-position** | **X-speed** | **Y-speed** |
|---|---|---|---|---|---|---|
| 1 | 1 | $EMG_1$ | $x_1$ | $y_1$ | $x'_1$ | $y'_1$ |
| 1 | 1 | $EMG_2$ | $x_2$ | $y_2$ | $x'_2$ | $y'_2$ |
| 1 | 2 | $EMG_3$ | $x_3$ | $y_3$ | $x'_3$ | $y'_3$ |
| 1 | 2 | $EMG_4$ | $x_4$ | $y_4$ | $x'_4$ | $y'_4$ |
| 1 | 2 | $EMG_5$ | $x_5$ | $y_5$ | $x'_5$ | $y'_5$ |
| 1 | 2 | $EMG_6$ | $x_6$ | $y_6$ | $x'_6$ | $y'_6$ |
| 1 | 2 | $EMG_7$ | $x_7$ | $y_7$ | $x'_7$ | $y'_7$ |
| 2 | 1 | $EMG_8$ | $x_8$ | $y_8$ | $x'_8$ | $y'_8$ |
| 2 | 1 | $EMG_9$ | $x_9$ | $y_9$ | $x'_9$ | $y'_9$ |
| 2 | 2 | $EMG_{10}$ | $x_{10}$ | $y_{10}$ | $x'_{10}$ | $y'_{10}$ |
| 2 | 2 | $EMG_{11}$ | $x_{11}$ | $y_{11}$ | $x'_{11}$ | $y'_{11}$ |
| 2 | 2 | $EMG_{12}$ | $x_{12}$ | $y_{12}$ | $x'_{12}$ | $y'_{12}$ |
| 2 | 2 | $EMG_{13}$ | $x_{13}$ | $y_{13}$ | $x'_{13}$ | $y'_{13}$ |
| 2 | 2 | $EMG_{14}$ | $x_{14}$ | $y_{14}$ | $x'_{14}$ | $y'_{14}$ |

Table 3.4: Example of the re-organization of the data: 14 first lines of the table.

We are now going to fit a linear mixed-effects model on our data. The random factor is the participant, the categorical factor is the trial, the kinematics variables are the fixed factors and the EMG is the variable that we want to explain. This analysis was made for each muscle and for each perturbation.

The p-values resulting from this analysis are summarized in tables 3.5, 3.6, 3.7, 3.8, 3.9 and 3.10, respectively for the biceps, the triceps, the anterior deltoid, the posterior deltoid, the pectoralis major and the infraspinatus. One can see that most of the p-values are superior to the significant threshold of $p = 0.05$. However, some of the tests are significant. For example, it appears that the difference between the EMG activities of the biceps for a clockwise perturbation can be explained by the x-position and the x-speed of the hand. On the other hand, the difference in the EMG curves of the triceps during clockwise trials can not be explained by any of the kinematics variables. There is not a clear repeated scheme through the tables.

| **Kinematics variable** | **CCW** | **CW** |
|---|---|---|
| X-position | 0.3940 | 0.0001* |
| Y-position | 0.6537 | 0.7871 |
| X-speed | 0.0194* | 0.0104* |
| Y-speed | 0.1857 | 0.4089 |

Table 3.5: P-values of the linear mixed-effects model for the biceps. *: $<$ p $= 0.05$

| Kinematics variable | CCW | CW |
|---|---|---|
| X-position | 0.0305* | 0.4582 |
| Y-position | 0.1243 | 0.7705 |
| X-speed | 0.2388 | 0.5496 |
| Y-speed | 0.8128 | 0.0508 |

Table 3.6: P-values of the linear mixed-effects model for the triceps. *: $< p = 0.05$

| Kinematics variable | CCW | CW |
|---|---|---|
| X-position | 0.7555 | 0.0685 |
| Y-position | 0.6687 | 0.2187 |
| X-speed | 0.3472 | 0.0416* |
| Y-speed | 0.5589 | 0.0089* |

Table 3.7: P-values of the linear mixed-effects model for the anterior deltoid. *: $< p = 0.05$

| Kinematics variable | CCW | CW |
|---|---|---|
| X-position | 0.0870 | 0.7726 |
| Y-position | 0.3862 | 0.9373 |
| X-speed | 0.0679 | 0.0455* |
| Y-speed | 0.2023 | 0.0012* |

Table 3.8: P-values of the linear mixed-effects model for the posterior deltoid. *: $< p = 0.05$

| Kinematics variable | CCW | CW |
|---|---|---|
| X-position | 0.4825 | 0.3678 |
| Y-position | 0.7538 | 0.4672 |
| X-speed | 0.1302 | 0.1164 |
| Y-speed | 0.1464 | 0.0147* |

Table 3.9: P-values of the linear mixed-effects model for the pectoralis major. *: $< p = 0.05$

| Kinematics variable | CCW | CW |
|---|---|---|
| X-position | 0.0064* | 0.7128 |
| Y-position | 0.3761 | 0.8126 |
| X-speed | 0.0644 | 0.0000* |
| Y-speed | 0.5767 | 0.0146* |

Table 3.10: P-values of the linear mixed-effects model for the infraspinatus. *: $< p = 0.05$

In order to push the analysis further, we now want to assess the relevance of the model used to fit our data. To do so, we fitted two other linear mixed-effects models to our data. We changed the fixed factors of the model, everything else stayed the same. The second model took the position (x and y-coordinates) as fixed factors while the third model only used an offset. For each muscle and for each perturbation, we then compared the BIC of the three models to see which one was the best. Table 3.11 summarizes the BIC of the three models, for each muscle and for each perturbation. One can see that the BIC decreases between the Offset and the Position column, for each muscle and for each perturbation. This indicates that considering the x and the y-positions as fixed factors in the model is relevant. If we now compare the Position and the

Position and Speed columns, there is not a constant evolution between the two models through the muscles and the perturbations. The model taking the x and y-positions and the x and y-speeds as fixed factors seems to be as relevant as the model taking only the x and y-positions as fixed factors.

| **Muscle and perturbation** | **Offset** | **Position** | **Position and Speed** |
|---|---|---|---|
| Anterior deltoid CCW | 468.5842 | 462.9695 | 464.2508 |
| Anterior deltoid CW | 386.7113 | 369.0148 | 355.5034 |
| Posterior deltoid CCW | 444.4759 | 429.1055 | 429.4135 |
| Posterior deltoid CW | 565.2521 | 559.7639 | 540.2281 |
| Biceps CCW | 362.2689 | 360.3421 | 358.9947 |
| Biceps CW | 365.9553 | 346.1067 | 345.7147 |
| Triceps CCW | 377.1258 | 363.3281 | 367.4169 |
| Triceps CW | 385.9842 | 382.6936 | 381.8566 |
| Pectoralis major CCW | 248.6634 | 247.3182 | 248.7562 |
| Pectoralis major CW | 193.0704 | 189.0107 | 185.001 |
| Infraspinatus CCW | 7.385671 | 2.536595 | 9.252785 |
| Infraspinatus CW | 236.8178 | 235.756 | 206.6656 |

Table 3.11: BIC of the three linear mixed-effects models for each muscle and for each perturbation. Second column: only use of an offset; third column: x and y-positions as fixed factors; last column: x and y-positions and x and y-speeds as fixed factors.

# Chapter 4

# Discussion

We asked participants to perform reaching movements and we randomly applied disturbing force fields during the trials. The perturbation could be either clockwise or counter-clockwise. The participants could not anticipate when a perturbation would occur and its direction.

## 4.1 Trajectory

We first examined the trajectories by looking at the maximum deviation along the x-axis and the overshoot. Our first result was that there was a clear evolution of the overshoot along the perturbed trials while the maximum deviation remained approximately constant. The maximum deviation did not decrease with the number of perturbed trials and this makes sense because the participants could not anticipate the perturbation. This also supports the idea that the diminution of the overshoot along the trials can not be explained by an anticipation of the force field. However, we saw that the behaviour of the overshoot could be fitted by an exponential model which is a typical learning curve. After about ten perturbed trials, the participants learned how to control their limb in order to overcome the perturbation and reach the target without doing an overshoot. Since they could not anticipate the perturbation, this supports the hypothesis that the participants modified their control strategy in real-time during the ongoing movement. This confirms the previous results of Frédéric Crevecoeur, Jean-Louis Thonnard and Philippe Lefèvre in their 2018 paper. [2]

## 4.2 Forces

We then compared the x and y-forces recorded at the handle of the robotic device for the first and the last perturbed trials, for both perturbations. In both cases, we saw that the second peak of the curve decreased between the first and the last perturbed trials. This is consistent with the diminution of the overshoot. Indeed, the force applied in the direction of the overshoot decreased, showing that the participants learned to exert a smaller force and avoided to go across the target. This result was also observed in the previous work of Frédéric Crevecoeur, Jean-Louis Thonnard and Philippe Lefèvre. [2]

## 4.3 EMG activity

### 4.3.1 Qualitative analysis

We analyzed the EMG activity of the biceps, the triceps, the anterior and posterior deltoids, the pectoralis major and the infraspinatus between the first and the last perturbed trials for both perturbations. Since we observed an evolution of the trajectory and the forces between the first and the last trial, we also expected to observe a difference in the EMG activity. We indeed saw that the EMG curves were qualitatively different between the first and the last perturbed trials, for both perturbations and for each muscle. At some point during the trial, the curve of the last perturbation was clearly located below the curve of the first perturbation, indicating a decrease in the EMG activity. We expected to observe this diminution since we observed a decrease at some point in the forces. The fact that the EMG curves differed at some point during the trial but not at the very beginning of the trial is another indication that the participants could not anticipate the perturbation but instead learned the dynamics of the perturbation and changed their on-line control strategy.

We then focused on pairs of muscles and we began with the pectoralis major and infraspinatus. Those muscles are responsible for two symmetric rotations of the arm. We observed a certain symmetry in their EMG curves while comparing the curves under a counter-clockwise and a clockwise perturbation. In other words, it looked like these two muscles had exchanged their behaviours when facing two symmetric perturbations. We also saw that after a brief period of co-contraction, the two muscles were synchronized in a certain way: one was inhibited while the activity of the other increased. We observed the same type of behaviour when we analyzed the anterior and posterior deltoids. We finally focused on the biceps and the triceps which are respectively responsible for the flexion and the extension of the forearm on the arm. We also observed a certain symmetry between the two muscles when comparing the curves of the two perturbations, even if it was less obvious than the symmetry observed in the pectoralis major and the infraspinatus. We also observed that each muscle showed a behaviour consistent with our expectations regarding their main actions and the perturbations applied. Indeed, the triceps, the posterior deltoid and the infraspinatus seemed to increase their activity before the biceps, the anterior deltoid and the pectoralis major during counter-clockwise trials and vice versa.

### 4.3.2 Critical times

We statistically objectified the difference of the EMG curves between the first and the last perturbed trials, for each perturbation and for each muscle. We then retrieved the critical times, defined as the moment at which the two curves became statistically different according to the p-values of a paired $t$-test. We reported these critical times on the mean trajectories of the last perturbed trials across participants and found that the critical times of the anterior deltoid and the pectoralis major occurred late in the trial, when the participant had already reached the target. We observed the same result in the biceps for clockwise trials. This result shows that the difference in the EMG activity of those two muscles can not explain the change of control strategy during the on-going movement. This change might be related to the stabilization of the hand once the target was reached. For the other muscles, the critical times occurred approximately when the trajectory reached its maximum deviation, i.e. before the participant had reached the target. The EMG activity of those muscles is consistent with the idea of an adaptive control to overcome unpredictable perturbations during reaching movements.

We then situated those critical times with respect to the beginning of the movement. The distribution of the starting times was centered around 900 ms. By looking at the critical times

and at the distribution of the starting times, we found that the changes in EMG activity occurred on average 375 ms after the beginning of the movement. This excludes the possibility that this change of behaviour is based on visual feedback or on spinal feedback loops, since they occur at shorter delays, respectively 150-250 ms and 30-50 ms. [11]

### 4.3.3 Statistical analysis

We objectified the difference of the EMG curves between the first and the last perturbed trials, for each perturbation and for each muscle by performing repeated-measures ANOVA. We found that as expected, the temporal mean of the EMG curves taken over 30 ms after the critical times significantly differed between the first and the last perturbed trials. This again supports the idea that at some point in the trial, the participants were able to modify their behaviour regarding the perturbation without any anticipation.

We then fitted linear mixed-effects models to our data in order to see if the kinematics of the movement (x and y-positions and x and y-velocities) could explain the difference observed in the EMG signals. We did it for each muscle and for each perturbation. We did not find any clear pattern that repeated itself across the muscles and the perturbations. For some cases, the difference in EMG activity could be explained by the position, for other cases by the velocity and sometimes neither kinematics variables could explain it. This indicates that the kinematics variables of the movement can not be solely responsible for the change observed in EMG activity between the first and the last perturbed trials. This is also consistent with the hypothesis that the CNS uses adaptive controllers to control and stabilize the upper limb during reaching movements.

We finally compared three different linear mixed-effects models to fit our data but the analysis of the BIC did not lead to a simple decision: indeed, both models (one using all kinematics variables and the other using only position variables as fixed factors) seemed appropriate to fit the data.

# Conclusion

The present work is a contribution to the understanding of the strategies established by the CNS to correct for disturbances during reaching movements in humans. The goal was to investigate if the CNS performs on-line corrections for perturbations following the principle of adaptive control.

18 participants performed reaching movements and force field perturbations were randomly applied during the trials. Our results confirmed the ones obtained in the previous paper of Frédéric Crevecoeur, Jean-Louis Thonnard and Philippe Lefèvre [2], and supported the hypothesis of an on-line learning of the dynamics. The investigation of the emg activity of muscles responsible for the movement of the shoulder and the elbow also supports this idea. Indeed, we found that the changes in EMG activity occurred on average 375 ms after the beginning of the movement and this change could not be systematically explained by the kinematics of the movement.

The original contribution of this manuscript is to show based on muscle recordings that the nervous system may alter its internal representation of movement dynamics within an ongoing movement, in less than 400ms on average. Our results are consistent with the hypothesis of an on-line learning and control of the upper arm in reaching movements when correcting for external perturbations. This should encourage others to further investigate this hypothesis, for example by analyzing the activity of other muscles or by studying the behaviour for a different paradigm of perturbation.

# Bibliography


[1] R. Shadmehr, F. A. Mussa-lvaldi. Adaptive Representation of Dynamics during Learning of a Motor Task. *The Journal of Neuroscience*, pages 74(5): 3208–3224, 1994. https://doi.org/10.1523/JNEUROSCI.14-05-03208.

[2] F. Crevecoeur, J.-L. Thonnard, P. Lefèvre. A sub-movement time scale of human motor adaptation. 2018. https://doi.org/10.1101/269134.

[3] Wikipedia. Motor adaptation, January 2018. https://en.wikipedia.org/wiki/Motor$_a daptation Accessed$ : 21/05/2018.

[4] D. A. Kistemaker, J. D. Wong, P. L. Gribble. The Central Nervous System Does Not Minimize Energy Cost in Arm Movements. *J Neurophysiol*, page 104:2985–2994, 2010. https://doi.org/10.1152/jn.00483.2010.

[5] M. Mistry, E. Theodorou, S. Schaal, M. Kawato. Optimal control of reaching includes kinematic constraints. *J Neurophysiol*, page 110:1–11, 2013. https://doi.org/10.1152/jn.00794.2011.

[6] J. Izawa, T. Rane, O. Donchin, R. Shadmehr. Motor Adaptation as a Process of Reoptimization. *The Journal of Neuroscience*, page 28(11): 2883–2891, 2008. https://doi.org/10.1523/JNEUROSCI.5359-07.2008.

[7] R. Shadmehr, M. A. Smith, J. W. Krakauer. Error Correction, Sensory Prediction, and Adaptation in Motor Control. *Annual Review of Neuroscience*, page 33:89–108, 2010. https://doi.org/0.1146/annurev-neuro-060909-153135.

[8] I. Doré Landau, R. Lozano, M. M'Saad, A. Karimi. *Adaptive Control: Algorithms, Analysis and Applications.* Springer, London, 2001. pages 1-33. https://doi.org/10.1007/978-0-85729-664-1.

[9] The Editors of Encyclopaedia Britannica. Control system, January 2018. https://www.britannica.com/technology/control-systemref199542 Accessed : 21/05/2018.

[10] C. Cao, L. Ma, Y. Xu. Adaptive Control Theory and Applications. *Journal of Control Science and Engineering*, pages vol. 2012, Article ID 827353, 2 pages, 2012. https://doi.org/10.1155/2012/827353.

[11] M. Kawato. Internal models for motor control and trajectory planning. *Current Opinion in Neurobiology*, page 9:718–727, 1999. https://doi.org/10.1016/S0959-4388(99)00028-8.

[12] E. Burdet, R. Osu, D. W. Franklin, T. E. Milner, M. Kawato. The central nervous system stabilizes unstable dynamics by learning optimal impedance. *Letters to nature*, page 414(6862):446–449, 2001. https://doi.org/10.1038/35106566.

[13] D. W. Franklin, G. Liaw, T. E. Milner, R. Osu, E. Burdet, M. Kawato. Endpoint Stiffness of the Arm Is Directionally Tuned to Instability in the Environment. *The Journal of Neuroscience*, page 27(29):7705–7716, 2007. https://doi.org/10.1523/JNEUROSCI.0968-07.2007.

[14] K. Singh, S. H. Scott. A motor learning strategy reflects neural circuitry for limb control. *Nature Neuroscience*, page 6:399–403, 2003. https://doi.org/10.1038/nn1026.

[15] M. J. Wagner, M. A. Smith. Shared Internal Models for Feedforward and Feedback Control. *The Journal of Neuroscience*, page 28(42):10663–10673, 2008. https://doi.org/10.1523/JNEUROSCI.5479-07.2008.

[16] I. Kurtzer, J. A. Pruszynski, S. H. Scott. Long-Latency Responses During Reaching Account for the Mechanical Interaction Between the Shoulder and Elbow Joints. *J Neurophysiol*, page 102: 3004–3015, 2009. https://doi.org/10.1152/jn.00453.2009.

[17] T. Cluff, S. H. Scott. Rapid Feedback Responses Correlate with Reach Adaptation and Properties of Novel Upper Limb Loads. *The Journal of Neuroscience*, page 33(40):15903–15914, 2013. https://doi.org/10.1523/JNEUROSCI.0263-13.2013.

[18] J. Y. Nashed, F. Crevecoeur, S. H. Scott. Rapid Online Selection between Multiple Motor Plans. *The Journal of Neuroscience*, page 34(5):1769–1780, 2014. https://doi.org/10.1523/JNEUROSCI.3063-13.2014.

[19] BKIN products. Kinarm end-point lab, January 2018. http://www.bkintechnologies.com/bkin-products/kinarm-end-point-lab/. Accessed : 30/04/2018.

[20] Yoganatomy. The biceps brachii muscle, September 2015. https://www.yoganatomy.com/the-biceps-brachii-muscle-2/. Accessed : 18/04/2018.

[21] Musculoskeletal Key. Triceps tendon ruptures, July 2016. https://musculoskeletalkey.com/triceps-tendon-ruptures/. Accessed : 18/04/2018.

[22] Myprotein. Musculation des épaules : Les 4 fantastiques pour les deltoïdes, April 2015. https://fr.myprotein.com/thezone/entrainement/musculation-des-epaules-les-4-fantastiques-pour-les-deltoides/. Accessed : 18/04/2018.

[23] TeachMeAnatomy. Muscles of the pectoral region, December 2017. http://teachmeanatomy.info/upper-limb/muscles/pectoral-region/. Accessed : 18/04/2018.

[24] Wikipédia. Muscle infra-épineux, March 2017. https://fr.wikipedia.org/wiki/Muscle_infra-épineux. Accessed : 18/04/2018.

[25] Delsys. Bagnoli surface emg sensor, January 2018. https://www.delsys.com/products/desktop-emg/surface-emg-sensors/. Accessed : 18/04/2018.

[26] Statistics How To. Bayesian information criterion (bic) / schwarz criterion, March 2018. http://www.statisticshowto.com/bayesian-information-criterion/ Accessed : 20/05/2018.

Rue Archimède, 1 bte L6.11.01, 1348 Louvain-la-Neuve **www.uclouvain.be/epl**